Accepted Manuscript

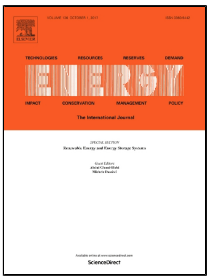

Selection of cooling fluid for an organic Rankine cycle unit recovering heat on a container ship sailing in the Arctic region

Santiago Suárez de la Fuente, Ulrik Larsen, Leonardo Pierobon, Martin R. Kærn, Fredrik Haglind, Alistair Greig

PII:	S0360-5442(17)31645-6
DOI:	10.1016/j.energy.2017.09.125
Reference:	EGY 11619
To appear in:	*Energy*
Received Date:	21 December 2016
Revised Date:	01 August 2017
Accepted Date:	25 September 2017

Please cite this article as: Santiago Suárez de la Fuente, Ulrik Larsen, Leonardo Pierobon, Martin R. Kærn, Fredrik Haglind, Alistair Greig, Selection of cooling fluid for an organic Rankine cycle unit recovering heat on a container ship sailing in the Arctic region, *Energy* (2017), doi: 10.1016/j.energy.2017.09.125

HIGHLIGHTS

- Air-cooling and seawater-cooling approaches are compared for marine ORC units.
- While navigating in the Arctic at least 471 t of CO_2 are reduced using an ORC unit.
- Air-cooled and seawater-cooled ORC units offer regulatory compliance to the vessel.
- Seawater is the preferable cooling fluid when maximum CO_2 reduction is wanted.

Selection of cooling fluid for an organic Rankine cycle unit recovering heat on a container ship sailing in the Arctic region

Santiago Suárez de la Fuente[a,*], Ulrik Larsen[b], Leonardo Pierobon[c], Martin R. Kærn[b], Fredrik Haglind[c], Alistair Greig[a]

[a] University College London, Department of Mechanical Engineering, Roberts Building, Torrington Place, London, WC1E 7JE, United Kingdom

[b] Chalmers University of Technology, Maritime Operations, 412 96 Gothenburg, Sweden

[c] Department of Mechanical Engineering, Technical University of Denmark, Building 403, Nils Koppels Allé, 2800 Kgs. Lyngby, Denmark

ABSTRACT

As Arctic sea ice coverage declines it is expected that marine traffic could increase in this northern region due to shorter routes. Navigating in the Arctic offers opportunities and challenges for waste heat recovery systems (WHRS). Lower temperatures require larger heating power on board, hence a larger demand for waste heat usage, to cover services and maintaining on board spaces temperatures. However, a lower heat rejection temperature increases the WHRS thermal efficiency. The air temperature for the Arctic route selected is colder than that of the seawater, opening the opportunity of having air as coolant. This paper explores the use of two different coolants, air and seawater, for an organic Rankine cycle (ORC) unit using the available waste heat in the scavenge air system of a container ship navigating in Arctic Circle.

Using a two-step single objective optimisation process, detailed models of air and seawater heat exchangers are evaluated as the WHRS condensers. The results suggest that an ORC unit using R1233zd(E) as its working fluid coupled with seawater as its coolant is the preferable option to reduce CO_2 emissions. Using the ambient air as the coolant while a less effective option could be cheaper to install.

Keywords: Organic Rankine cycle, Arctic shipping, Waste heat recovery, Condensers, CO_2 emissions.

* Principal corresponding author. *Email address*: santiago.fuente.2011@ucl.ac.uk (Santiago Suárez de la Fuente)

NOMENCLATURE

Symbol	Name	Units	Symbol	Name	Units
A	Area	m^2	n	Shell type heat exchanger's constant	-
BP	Bypass	%	N_t	Number of tubes	-
CE	Carbon emissions	t/h	N_{tpr}	Number of tubes per row	-
CS	Carbon savings	t/h	N_{tr}	Number of tube rows	-
C_F	Carbon factor	t CO_2/t fuel	Nu	Nusselt number	-
c_p	Specific heat at constant pressure	kJ/kg·K	OM	Number of months	-
C_p	Prismatic coefficient	-	OS	Number of operating speeds	-
C_m	Midship section coefficient	-	p	Pitch	mm
d	Diameter	m	P	Pressure	kPa
EEDI	Energy Efficiency Design Index	g CO_2/t·nm	Pr	Prandtl number	-
F	Correction factor	-	$\dot{Q}$	Heat transfer rate	kW
FS	Fuel savings	t/h	Re	Reynolds number	-
g	Gravitational acceleration	m/s^2	$SFOC$	Specific fuel oil consumption	g/kWh
h	Specific enthalpy	kJ/kg	t	Time	h
h^*	Convective heat transfer coefficient	$kW/m^2·K$	T	Temperature	K
l	Length	m	TW	Transport work	t·nm
K	Shell type heat exchanger's constant	-	U	Overall heat transfer coefficient	$kW/m^2·K$
$\dot{m}$	Mass flow rate	kg/s	v	Speed	m/s
M	*Mass flow rate ratio*	-	V	Volume	m^3
MT	Monthly trips	-	$\dot{W}$	*Power*	*kW*
Greek Symbol	**Name**	**Units**	**Greek Symbol**	**Name**	**Units**
ρ	Density	kg/m^3	η	Efficiency	%
Δ	Difference	-	K	Thermal conductivity	kW/m·K
μ	Dynamic viscosity	Pa·s			

Subscripts and superscripts	Name	Subscripts and superscripts	Name
ap	Approach	*lm*	Logarithm mean
b	Baffle	*me*	Maine engine
B	Bundle	*min*	Minimum
C	Cold side	*o*	Outlet/Outside
cf	Crossflow	*off*	Off-design
cl	Clearance	*p*	Pump/Pitch
co	Condenser	*pp*	Pinch point
cr	Critical	*r*	Reduced
cs	Cross sectional	*s*	Shell/Isentropic
d	Design	*S*	Air/Seawater/Sink
ds	Desuperheating	*sat*	Saturation
e	Hydraulic	*t*	Tube/Thickness
ex	Expander	*T*	Total
f	fin/fouling/friction	*tr*	Transversal
h	Height	*v*	Vapour
H	Hot side	*w*	Wall
ht	Heat transfer	*wf*	Working fluid
i	Inlet/Inside/Capacity	*WH*	Waste heat
j	Power	*WHRS*	Waste heat recovery system
l	Liquid		

1. INTRODUCTION

In the last decades, the ice coverage in the Arctic has been constantly declining. During the period between 1981 and 2010, an average decline of 4.9% in ice coverage has been observed in each decade [1]. This has opened the door for shorter shipping routes via the Arctic [2–4]. For example, the Rotterdam-Yokohama route through the Suez Canal is about 20,600 km, while the same route via the Arctic is only around 8,500 km [5]. Winther et al. [3] predicted that the shipping activities above the 59°N latitude will grow from 133.5 million km in 2012 to 208.7 million km by the year 2050, an increase of more than 55%. The largest increase in the same time frame is for container ships at around more than 300%, increasing from 6.8 million km to around 28.5 million km. Furthermore, Smith et al. [6] state that in order to avoid a global mean temperature rise of 2°C before 2100, the shipping industry needs to half its 2012 operational CO_2 emissions by 2050 and achieve zero emissions or neutrality in the year 2080. The shipping industry, in order to comply with this aggressive aim, is required to develop green and energy efficiency technologies and strategies, such as waste heat recovery systems (WHRS).

The largest source of waste heat from a ship's main engine is found in the exhaust gases, but the ambient air's low temperature in the northern region translates into a larger ship heat demand to ensure satisfactory operation of equipment and machinery (e.g. main engine lubricating oil should not be below the minimum temperature recommended by manufacturer) [7]. Depending on the type of ship and its size, the heating requirement is fully or partially covered by a waste heat boiler (WHB) using the exhaust gas waste heat and hence, in some cases, it is not feasible to use this heat source for other purposes [8]. Súarez de la Fuente [9] showed that for a large container ship the available waste heat in the exhaust gas would not be enough to cover the heating demand when the ambient air temperature is below 3°C. Another source of heat waste is found in the scavenge air after compression which represents around 15% of the fuel energy used [10,11]. The low temperature of the scavenge air, between 130°C and 150°C [12], is not attractive for power generation using the traditional water-based Rankine cycle units [13,14]. Organic Rankine cycle (ORC) technology presents a viable option to exploit scavenge air waste heat on board for power generation [15,16], but the behaviour of ORC WHRS in Arctic routes has not been studied in the existing literature.

The annual average temperatures in the Arctic is much lower than those in other oceans; from a thermodynamic cycle point of view this is an area of opportunity since the WHRS thermal efficiency increases due to a lower average temperature of heat rejection (see the Carnot efficiency [17]). Stanzel et al. [18] explored the use of an extra radiator for a heavy-duty truck air-cooled ORC unit to lower the unit's sink temperature. They found an increase in the ORC unit power return when using the extra radiator of about 2% and 25% at low and high-loads respectively, giving a fuel consumption improvement of about 0.6 percentage points. Alternatively, by increasing the pinch point temperature difference between the working and cooling fluids while keeping the working fluid condensation pressure, the temperature rise of the cooling fluid may be increased and the hence mass flow rate of the cooling fluid may be reduced, causing a reduction in pump/fan power consumption. Seawater

(SW) can be as cold as -2˚C [19] while ambient air can reach -37˚C [20,21]. The annual average air temperature can be as low as -12.0˚C[1] in navigable waters. The cold air opens an interesting area of research in relation to marine WHRS which is the use of an air condenser unit[2] instead of the typical seawater condenser unit. In a land-based system some of the strengths of air-cooled condenser units are its low cost and reduction in water requirement [22,23]. For the ship case in the Arctic using air as a coolant, in addition to the aforementioned performance benefits, the effects of seawater bio-fouling may be eliminated and, depending on the location of the heat exchanger, requiring less corrosion-resistant materials since seawater is not directly in contact with the heat exchanger material [24,25]. On the other hand, due to air's lower heat transfer coefficient and specific heat, there will be a need for larger heat transfer areas and volumetric flows in order to accomplish the cooler's heat rejection [26].

Zahi and Rubin [27] found that to achieve a 550 MW net power output for a pulverized coal power plant cooled by water the plant needs to produce a gross output of 593 MW while when using air cooling this increases to 601 MW. The power difference is due the greater auxiliary power required by for fans in air cooled plant compared to the pumps in the water cooled plant. Habl et al. [28] explored the differences of air and water as coolant for a 50 MW solar power plant located at the south of Spain and found that by using air the electricity cost increased by around 5%. He et al. [29] compared three different methods to reject excess heat from a particular cooling tower located in Australia for temperatures up to 35°C: Natural dry-air draft, pre-cooled natural dry-air draft and natural wet-air draft. It was found that the natural wet-air draft approach was capable of rejecting up 3 times more heat than the dry-air approach, but at the expense of high usage of water.

Bustamante et al. [26] recognise that by using air-cooled condenser units on a 500 MW power plant there will be a penalty between 5% and 10% in plant-level efficiency due to the extra auxiliary power required. In addition, they explored new heat transfer enhancement techniques, such as winglet vortex generators and passive chaotic mixing, to match the performance of water-cooled condenser units. Usman et al. [30] studied the performance change of a geothermal-powered ORC unit cooled either by air or cooling tower for different locations and seasons of the year. They found that the better cooling strategy for an ORC unit in a hot and dry climate is the cooling tower due to its higher net power output – around 16% – while air is a more attractive solution for colder regions due to a reduction in the power consumption of the condenser.

The aim of this paper is to find the most suitable combination of working and cooling fluids for a marine ORC unit using the available waste heat in the scavenge air system of a container ship navigating in the southern region of the Arctic Circle. The objective is to reduce the ship's operational annual CO_2 emissions while achieving energy efficiency design index regulation compliance. A two-step single-objective optimisation of different marine ORC WHRS and their condenser units is undertaken in order to observe their performance and environmental impact on board a ship capable

[1] This is the annual averaged temperature including anomalies for the South of Greenland adjacent to the Denmark Strait.

[2] In this paper, condenser unit refers to the whole heat exchanger, and condenser to the two-phase section inside the condenser unit.

of carrying 4,130 twenty-foot containers (TEU). This is the first paper addressing the use of air as cooling fluid in a marine ORC-based WHRS. The paper contributes to a highly relevant, previously unexplored area in marine engineering by studying the performance of marine WHRS in extremely cold weather and how these systems can reduce CO_2 emissions in delicate cold regions such as the Arctic.

The paper explains in section 2 the features of the system and the case study used. Section 3 outlines the methods used and section 4 goes on to compare the different working and cooling fluids combinations and then discusses their impacts on ship performance and the environment. Section 5 outlines the main conclusions.

2. SHIP SYSTEM DESCRIPTION

2.1 THE SHIP AND THE ARCTIC ROUTE

This paper studies the effects of the Arctic temperature in a marine WHRS on board a container ship navigating between Reykjavik, Iceland and the port of Ballstad in Norway as indicated in Figure 1. The region studied has latitude that goes from 62.5˚N to 67.5˚N and longitude from 22.5˚E to 12.5˚E with its respective annual average temperature profile for air (Figure 2) and seawater (Figure 3) taken from CRUTEM4 and HadSST2 data sets [19–21]. The route is 1,980 km and chosen due to its low temperatures, the fact that it is open for navigation the whole year, and finally because of data availability from commercial shipping which can bring a more realistic scenario.

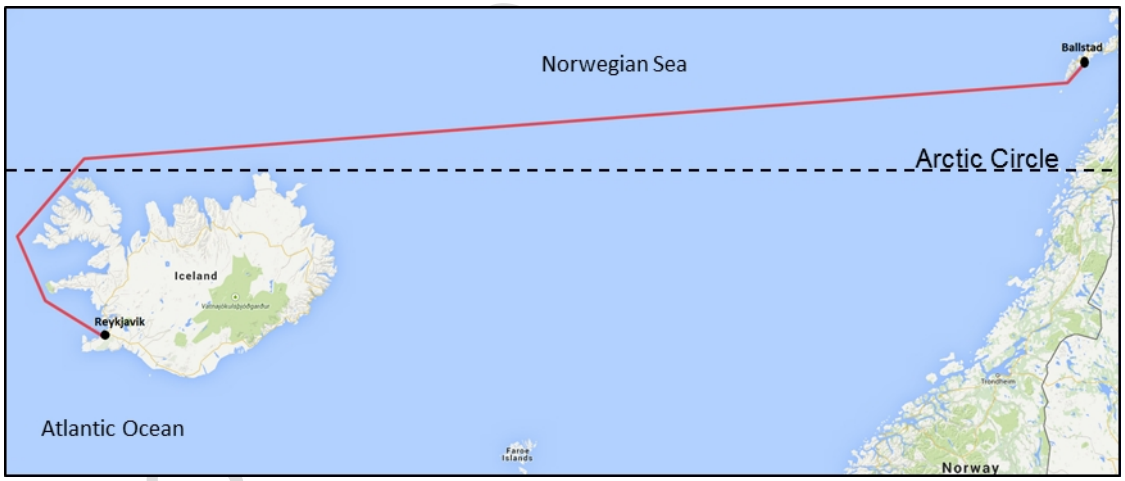

Figure 1: Representation of the route taken by a container ship between Iceland and Norway. A single trip has a distance of about 1,980 km [31].

A hypothetical container ship is selected for the case study. The ship can carry 4,130 TEU with a design speed of 23.3 knots (12.0 m/s) and a maximum speed of 25.2 knots (13.0 m/s) [32,33]. The operational profile for the container ship is shown in Figure 4 and was obtained using anonymised Automatic Identification System data from containerships navigating in the Arctic Ocean in the year

2012[3]. From the work of Banks et al. [34], the container ship will spend around 66% of the year fully loaded. The rest of the time is spent loading/unloading containers or in maintenance. Considering this operating profile, a single trip will take about 55 hours which means that the ship will be able to complete 104 single trips each year. It is assumed that the ship will have an operational life of 20 years. The ship's power-speed characteristics was obtained using data from Table 1 and Holtrop and Mennen resistance model [35] with corrections in Holtrop [36]. The ship's operational profile and route are integrated in a single function which assigns the proportional time of each speed seen in Figure 4 to a single voyage.

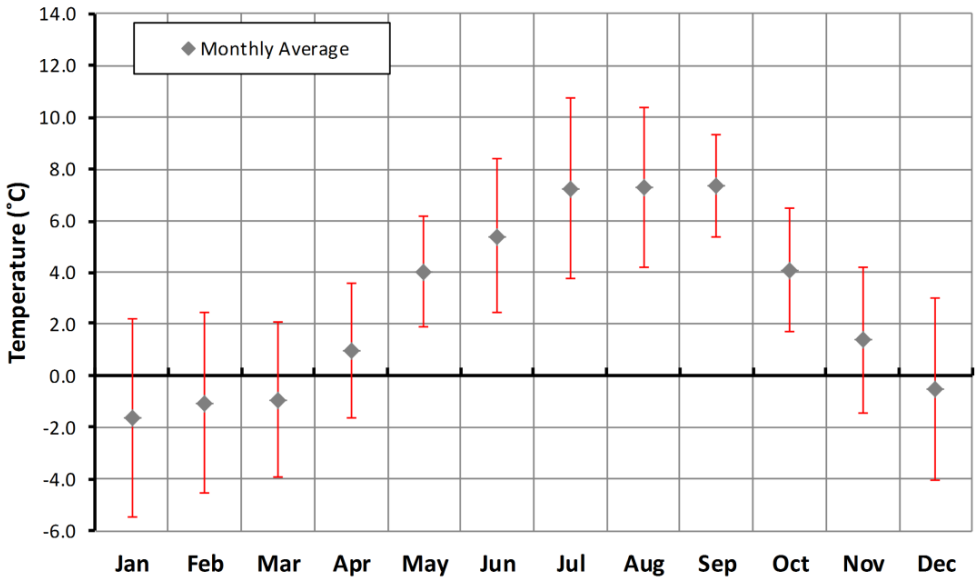

Figure 2: Ambient air temperatures for the region where the container ship will be navigating. The bars on both figures represent the temperatures' standard deviation.

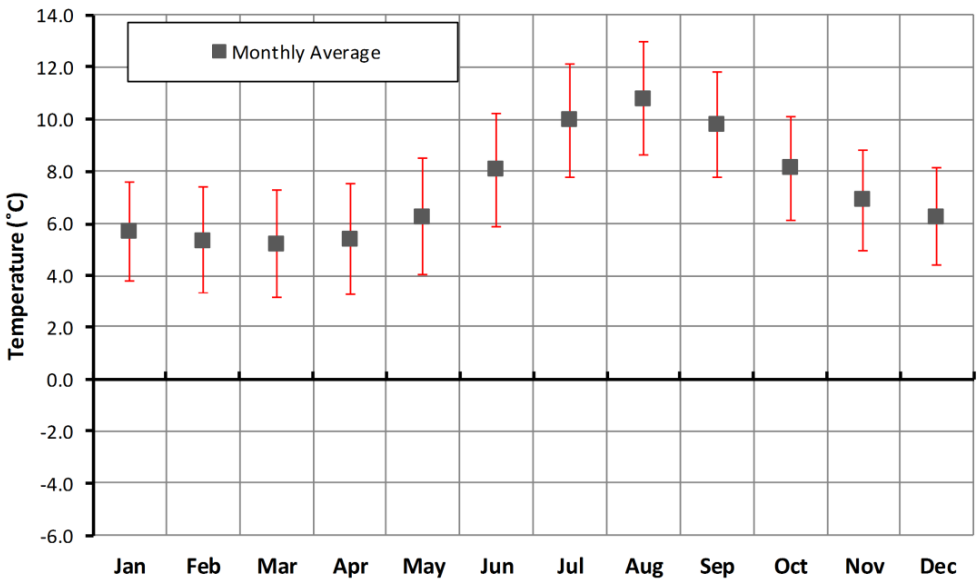

Figure 3: Monthly seawater temperatures for the region where the container ship will be navigating. The bars on both figures represent the temperatures' standard deviation.

[3] Data provided and processed by UCL's Energy Institute.

Since the ship will be navigating within the limits of the Arctic Circle, where the ambient temperatures are not lower than -15˚C, its winterisation level would be basic according to Det Norske Veritas (DNV) AS [37].

Table 1: Container ship's characteristics used for the case study [32,33]**.**

Deadweight (t)	*Length (m)*	*Beam (m)*	*Draught (m)*	*Midship Coefficient*[a] (-)	*Prismatic Coefficient*[b] (-)
52,450	252	32.2	12.5	0.981	0.653

[a] **Ratio of ship's underwater area at the midship section to that of the circumscribing rectangle** [38]**.**

[b] **Ratio of ship's underwater volume to the product of the area at the midship section and length** [38].

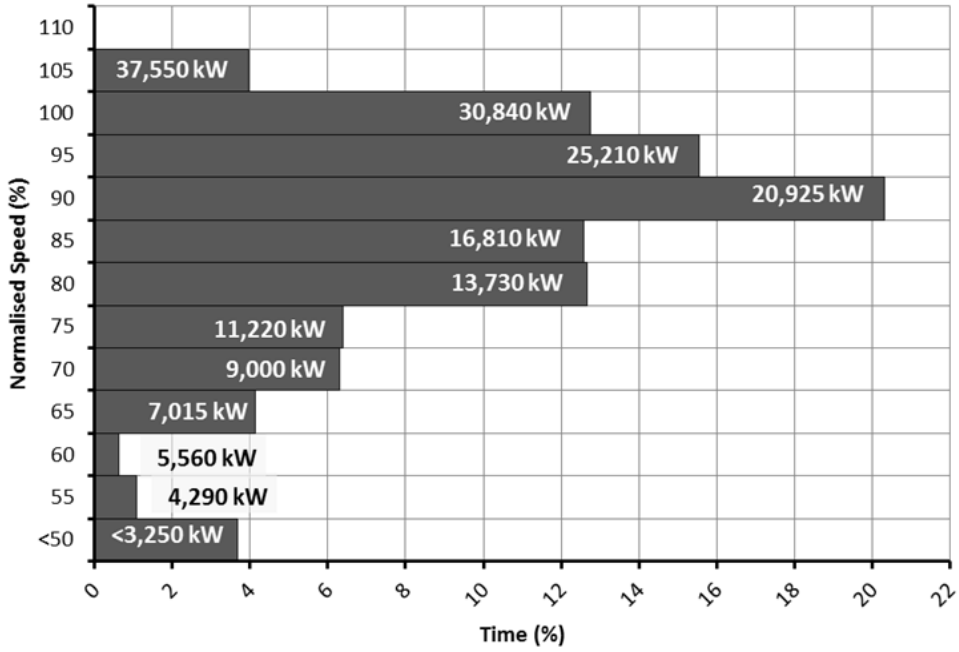

Figure 4: Annual operating profile for a container ship navigating in the Arctic Circle between the Norwegian Sea and Atlantic Ocean. The speed profile is normalised to the ship's design speed which is 23.3 knots.

2.2 MAIN ENGINE

The ship is powered by a two-stroke slow speed diesel engine using Heavy Fuel Oil (HFO). The engine is capable of delivering a maximum of 41,125 kW with specific fuel oil consumption (SFOC) of 163 g/kWh [39].

The design point – design speed – is set at 75% Maximum Continuous Rating (MCR) with a power output of 30,840 kW with SFOC of 159 g/kWh. The waste heat availability and temperature from the scavenge air increases almost linearly with the change of engine loading (see Figure 5). When fixing the engine's loading, it is seen from manufacturer's data (MAN Diesel and Turbo [39]) that there is a

4 kW decrease per degree Celsius in the scavenge air waste heat availability when the ambient air temperature increases from 10°C to 45°C.

The International Maritime Organization (IMO) is the United Nations agency that deals with all maritime matters including safety and pollution. It has created a worldwide, legally binding energy-efficiency measure for new-build ships called the Energy Efficiency Design Index (EEDI) which entered into force at the beginning of 2013 [40]. As part of the EEDI a series of baselines were established for the amount of CO_2 emitted by different types of ships and cargo capacity. The baselines get progressively more stringent over time – for example the EEDI baseline will reduce CO_2 emissions between 15% and 20%, depending on the type of ship, from the 2013 baseline. From the data in Table 1, the hypothetical new build ship studied in this work has an EEDI of 17.753 g CO_2/t-nm which is above the allowed EEDI 2015 reference value for this ship type, size and class is 17.647 g CO_2/t-nm [41]. To bring the ship below the 2015 reference value a mitigation measure must be added to the ship, for example the ORC WHRS proposed in this paper.

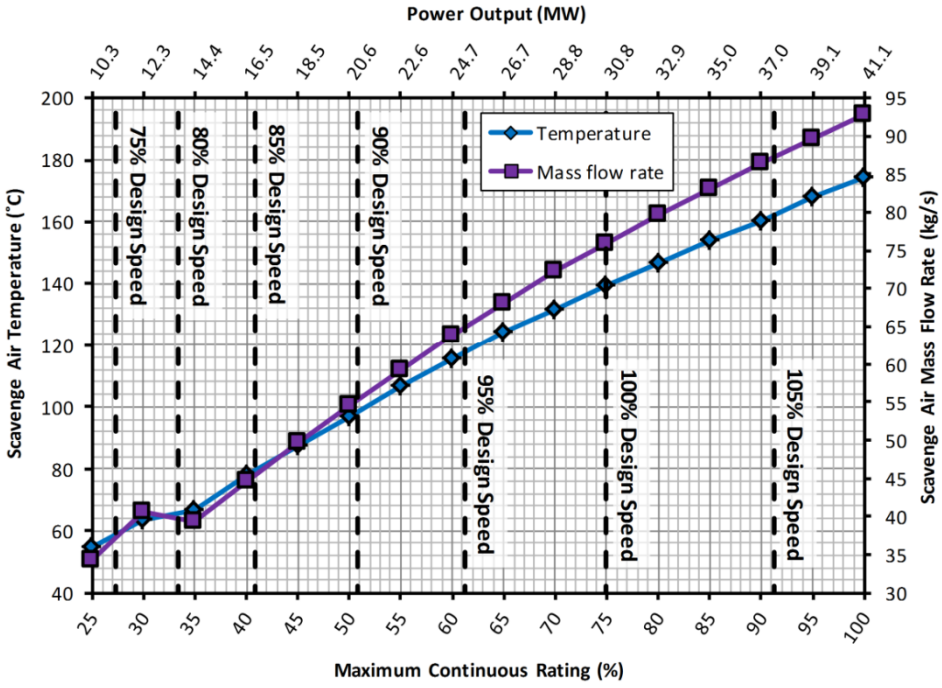

Figure 5: Temperature and mass flow rate after the inlet air is compressed for main engine [39].

2.3 WASTE HEAT RECOVERY SYSTEM

The location of the waste heat recovery system is shown in Figure 6. Cold air enters the compressor of the turbocharger which increases its pressure but also its temperature which in turn reduces air density. In order to allow for a larger mass of air into the engine's cylinders, the air's temperature is reduced using a heat exchanger, commonly known as intercooler or aftercooler [42], effectively increasing the charged air density. In this work it is proposed that the compressed air temperature is cooled via the WHRS boiler before it enters the main engine. The power produced by the WHRS is delivered to the main engine's shaft reducing the engine's fuel consumption and hence CO_2

emissions. The pressure losses due to the WHRS boiler are assumed to be the same as with a typical scavenge air heat exchanger. Pressure drops in the scavenge air are normally small, in the range of 1.0 Pa to 3.5 Pa [43] which has a small influence on the main engine performance and hence can be omitted [44]. It is also assumed that there will be an auxiliary heat exchanger after the WHRS which will cool the compressed air when the WHRS is off-line (e.g. at slow speeds).

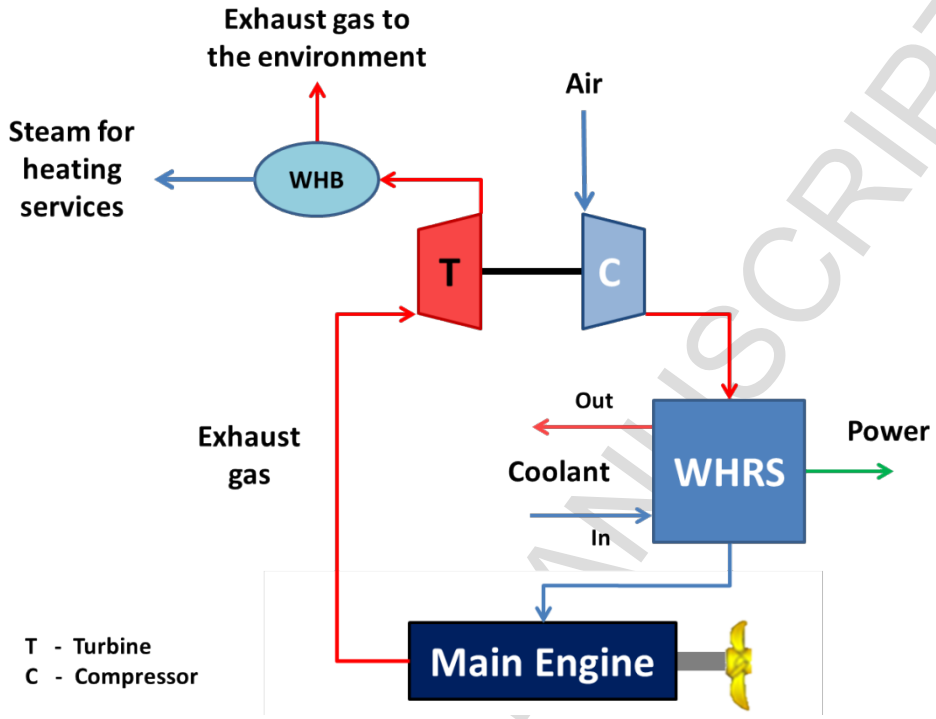

Figure 6: Sketch of the propulsion system layout using a WHRS on the scavenge air side. The layout also considers the use of a Waste Heat Boiler (WHB) on the exhaust gas after the turbocharger to cover the heating requirements when navigating in cold waters.

The waste heat boiler (WHB) exploits the exhaust gas waste heat and contributes to maintaining operational temperatures for machinery and other equipment throughout the ship when in cold climates [7]. The WHB would be in competition for a WHRS located on the exhaust side of the main engine.

The study of how the main engine performance is affected by colder temperatures, as well as the design and behaviour of the compressor at different engine loadings and air temperatures and the design of the auxiliary heat exchanger are outside of the scope of this paper. Similarly, the design of the WHB and impact of using a WHB is beyond the scope of this paper, a detailed study of the usage of WHB on board a container ship can be found in [9].

The working fluids studied are R1233zd(E), R236fa, R236ea and R245fa (see Table 2 for their properties and classification group). These four organic fluids were selected because they can operate under the waste heat scavenge air temperature profile shown in Figure 5 [45,46] and also because they are classified per National Paint Association's Hazardous Materials Identification System (HMIS) as non-flammable – classified as zero. This permits, as per International Maritime

Table 2: Working fluids selected with their global warming potential value in a time interval of 100 years (GWP_{100}); ozone depletion potential (ODP); auto-ignition, and decomposition temperatures; flammability classification; and critical temperature (T_{cr}) and critical pressure (P_{cr}).

Working Fluid	Fluid Group[a]	GWP_{100} [b]	ODP [c]	Auto-ignition Temperature (˚C)[d]	Decomposition Temperature (˚C)[e]	HMIS flammability [f]	T_{cr} (˚C)[g]	P_{cr} (MPa)[g]
R1233zd(E)	Hydrochlorofluoroolefin	<5	0.0	380	175	0	167	3.62
R236ea	Hydrofluorocarbon	1,596	0.0	N/A*	N/A	0	139	3.50
R236fa	Hydrofluorocarbon	8,060	0.0	N/A*	400	0	125	3.20
R245fa	Hydrofluorocarbon	950	0.0	412	250	0	154	3.65

[a] R1233zdE:[47]; R236ea, R236fa and R245fa: [48].

[b] R1233zdE: [49]; R236ea and R236fa: [50]; R245fa:[51].

[c] R1233zdE: [49]; R236ea: [52]; R236fa: [53]; R245fa: [54].

[d] R1233zdE: [55]; R245fa:[54].

[e] R1233zd(E): [56]; R236fa: [57]; R245fa: [54].

[f] R1233zdE: [55]; R236ea and R245fa: [45]; R236fa: [58].

[g] Taken from: [59].

* Auto-ignition tests are not applicable for these fluids since the vendors consider them as gases, hence ISO 2719 and ASTM D1310 does not apply.

Organization (IMO) Safety Of Life At Sea (SOLAS), their presence without further safety measures inside the machinery room [60], minimising the WHRS investment cost and resulting in a compact installation. Some do have the drawback of a significant global warming potential (GWP_{100}) making them probable candidates for future restrictions on board. Mondejar et al. [61] highlights the implications of new fluid regulation on high GWP_{100} fluids and propose the usage and research of hydrofluoroolefins such as the R1233zd(E). In the meantime and in order to mitigate the risk of leakages and high concentration of the refrigerant, the marine WHRS designer could use the guidelines and requirements for highly flammable fuels provided by IMO's [62] International Code of Safety for Ships using gases or other low flashpoint fuels and the Det Norske Veritas [63] tentative regulation as explored by Suárez de la Fuente et al. [64].

3. METHODS

3.1 MODELLING THE WASTE HEAT RECOVERY SYSTEM

Figure 7 shows the ORC unit layout which is suitable for low quality heat sources, such as that found in the scavenge air system [45]. The usage of a recuperator for the working fluid's flow after the expander and pump brings little benefit due to the low temperatures at the exit of the expander while increasing the volume and cost of the ORC unit.

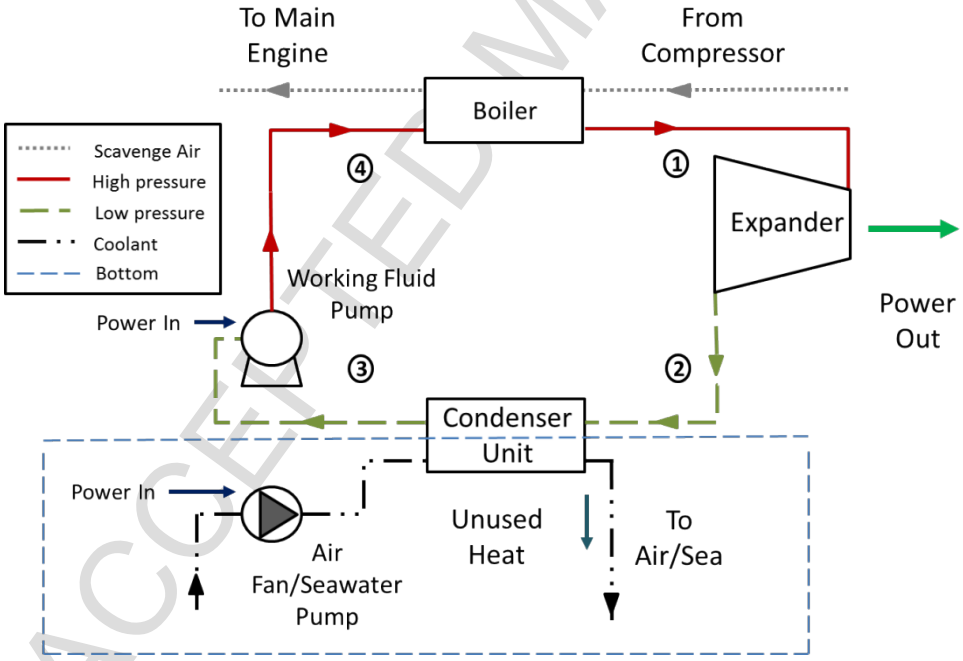

Figure 7: Simple plant layout for a marine ORC using the available waste heat after the air compression in the scavenge air system.

As mentioned in section 2.3 the WHRS boiler is used to cool the engine's charge air. Referring to Figure 7 and the WHRS is operating at the design point, the hot and high pressure air enters the WHRS once-through boiler where the excess heat is transferred to the working fluid (4-1), increasing its temperature. The waste heat absorbed by the ORC unit ($\dot{Q}_{WH}$) was calculated as follows:

$$\dot{Q}_{WH} = \dot{m}_{WH} BP c_{p,WH} (T_i - T_o) \quad (1)$$

Where is the mass flow rate ($\dot{m}_{WH}$), *BP* is the scavenge air mass bypass percentage to the auxiliary air cooler, $c_{p,WH}$ is the scavenge air specific heat, T_i and T_o are the scavenge air inlet and outlet temperature respectively. The $\dot{m}_{WH}$ at the different operating points were taken from [39], while T_o, *BP* and the design point for the ORC unit were chosen by the optimisation process. Table 3 presents the operating parameters for the ORC unit of which they are fixed or are chosen by the optimisation process.

The specific enthalpy of the working fluid after the boiler (h_1) was found using the superheating temperature and working fluid pressure after the boiler (P_1) which were selected by the optimisation process. The saturation temperature at low pressure – point 3 – was fixed at 25°C. The advantage of fixing the saturation temperature is that it allows the WHRS to operate up to ambient temperatures – seawater or air – close to 20°C when considering the 5°C minimum pinch point temperature difference. Also this saturation temperature constraint reduces the power consumption due to the larger pinch point temperature difference which allows for lower coolant mass flow rates. On the other hand, there is a cost to the expander's work output since it operates at a pressure which is not as low as it would otherwise be, this in turn reduces the pressure/enthalpy drop of the expansion process. With the assumption it is possible to find P_3 and the working fluid's saturation specific enthalpy (which under the assumption is also h_3).

Table 3: Operating characteristics explored by this study.

Parameter	Cooling Fluid	Range	Variable selection
Scavenge Air Outlet Temperature (˚C)	Air/SW	50 - 175	Optimisation
***BP* (%)**	Air/SW	0 – 75	Optimisation
P_1 (kPa)	Air/SW	300 – 0.95*P_{cr}	Optimisation
Superheating Temperature (˚C)	Air/SW	5 – 100	Optimisation
$\Delta T_{pp,s}$ (˚C)	Air/SW	5 – 25	Optimisation
WHRS Design Point (Ship Speeds)	Air/SW	75% -105% of Design Speed (27% - 91% MCR)	Optimisation
Design isentropic efficiency pump (%)	Air/SW	80	Fixed
Design isentropic efficiency expander (%)	Air/SW	80	Fixed

The isentropic efficiency of the pump (η_p) was used to find the working fluid specific enthalpy after the pump (h_4):

$$h_4 = h_3 + \frac{(h_{4s} - h_3)}{\eta_p} \quad (2)$$

Where h_{4s} is the specific enthalpy after the pump assuming an isentropic increase of pressure from P_3 to P_4 (i.e. P_1). By using the available waste heat going through the WHRS boiler, it was possible to find the working fluid's mass flow rate ($\dot{m}_{wf}$):

$$\dot{m}_{wf} = \frac{\dot{Q}_{WH}}{(h_1 - h_4)} \quad (3)$$

After the heat exchange process in the boiler the high pressure and temperature working fluid enters the turbine (1) and expands, providing mechanical power. The specific enthalpy after expansion (h_2) can be found using the definition of the isentropic efficiency of the expander:

$$h_2 = h_1 + \eta_{ex}(h_{2s} - h_1) \quad (4)$$

Where η_{ex} is the expander's isentropic efficiency, h_{2s} is the specific enthalpy after an isentropic expansion process with a change of pressure from P_1 to P_2. Then the power produced by the expander ($\dot{W}_{ex}$) was given by:

$$\dot{W}_{ex} = \dot{m}_{wf}(h_2 - h_1) \quad (5)$$

The condenser unit (2-3) then condenses the working fluid at constant pressure by rejecting heat to the sink, having at the end of the process a saturated liquid. The total heat rejected to the sink ($\dot{Q}_{co}$) is calculated as follows:

$$\dot{Q}_{co} = \dot{m}_{wf}(h_3 - h_2) \quad (6)$$

In order to fully comprehend the implications and differences between the two dissimilar cooling fluids, detailed models of the different condenser units are given in section 3.1.1. After the condenser unit, the working fluid's pressure is increased by the pump. The power consumed ($\dot{W}_p$) is given by:

$$\dot{W}_p = \dot{m}_{wf}(h_4 - h_3) \quad (7)$$

Closing the ORC unit loop, the working fluid is sent back to the boiler (4). Since the independent variables of this work are selected by the optimisation process, it is required to perform energy and mass flow balances as well as temperature profiles to observe that the ORC unit complies with the First Law of Thermodynamics and heat transfer phenomena.

A detailed description of the WHRS thermodynamic model – points 1 to 4 in Figure 7 – is provided as in Larsen et al. [45], Pierobon et al. [65] and Suárez de la Fuente & Greig [66]. The model was coded in Matlab® 2015a and it was coupled with CoolProp 5.0 [67] for the working fluid equations of state.

3.1.1 CONDENSER UNIT

When using seawater as a coolant the great flexibility in design and operational conditions, and ease of maintenance makes shell and tube heat exchangers the preferred choice as the WHRS condenser unit [68]. Flow inside the tube is recommended for the most corrosive fluids, but is also recommended for liquids. The tube layout was assumed to be a rotated square – same pitch between adjacent tubes

– which gives high heat transfer rates but with a larger pressure drop from the working fluid side [68]. Due to the corrosive nature of seawater, the condenser unit would be constructed using stainless steel.

When using air as coolant a finned tube condenser unit was used. This type of heat exchanger offers higher heat transfer area densities – up to around 3,300 m^2/m^3 – than a shell and tube heat exchanger, reducing the condenser unit's mass and volume [69]. The fins used were of circular construction with an annular layout on the tube (i.e. perpendicular to the tube surface) and were of the same material as the tubes. The maintenance on the finned side could become burdensome and it is recommended that the least corrosive fluid with the lowest tendency to foul flows in this section, which in this case is the air. This decision also made sense from the overall heat transfer coefficient (U) point of view since air is flowing in the section of the condenser unit that offers the largest contact area which is beneficial when having a low convective heat transfer coefficient (h^*). The finned tube condenser unit was made of aluminium with five tube rows with a rotated square layout with a constant transverse pitch (p_t) of 83 mm [22]; the working fluid flowing inside the tubes had a maximum speed of 15 m/s. The governing equation for the heat transfer across a surface using the condenser unit's desuperheating section (ds) shown in Figure 8 was given by:

$$\dot{Q}_{ds} = U_{ds} A_{ds} F_{cf} \Delta T_{lm,ds} = \dot{m}_{wf}\left(h_2 - h_{2a}\right) \quad (8)$$

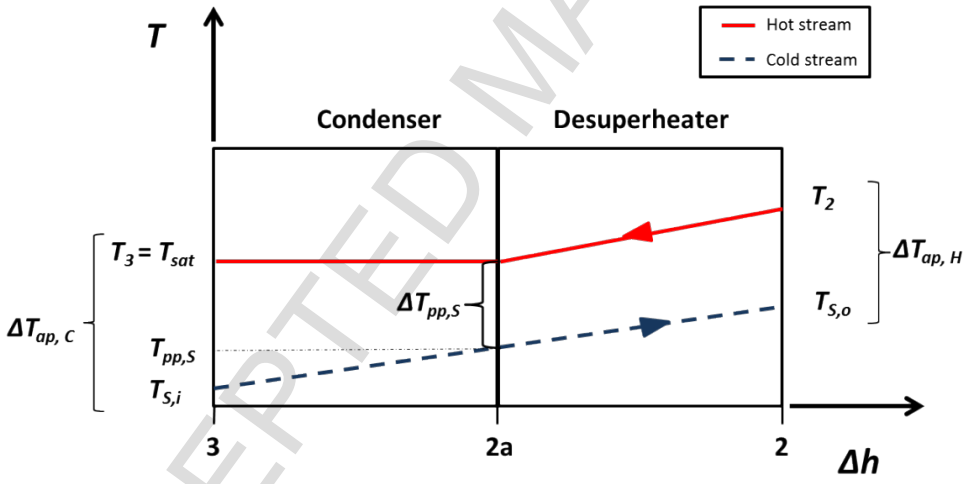

Figure 8: Representation of the condenser unit and its two subsections in a *temperature (T) versus change in enthalpy* (Δh) plot. The cold side approach temperature ($\Delta T_{ap,C}$) in the condenser unit is defined as the temperature difference between the working fluid saturation temperature (T_{sat}) and the heat sink inlet temperature ($T_{S,i}$).

where $\dot{Q}$ is the heat rate, U is the overall heat transfer coefficient, A is the heat transfer area and F_{cf} is the temperature correction factor which accounts for the deviation of the flow shape inside the condenser unit from an ideal counter current flow and was calculated using the correlations given in the different references found in Table 4. The h_{2a} is the working fluid's specific enthalpy at its saturated vapour state when the pressure is P_3. The ΔT_{lm} is the logarithm mean temperature difference and was calculated for the counter flow desuperheater section as follows:

$$\Delta T_{lm,ds} = \frac{(T_2 - T_{S,o}) - (T_{sat} - T_{pp})}{ln\left(\frac{T_2 - T_{S,o}}{T_{sat} - T_{pp}}\right)} = \frac{\Delta T_{ap,H} - \Delta T_{pp,S}}{ln\left(\frac{\Delta T_{ap,H}}{\Delta T_{pp,S}}\right)} \quad (9)$$

Where $\Delta T_{ap,H}$ is the hot side approach temperature defined by the difference between the expander outlet temperature (T_2) and the outlet temperature of the cooling fluid ($T_{S,o}$). The pinch point temperature difference ($\Delta T_{pp,S}$) is given by the difference between T_{sat} (i.e. T_3) and the pinch point temperature ($T_{pp,S}$) found at point 2a.

The overall heat transfer coefficient, when seen from the outside of a finned tube in the desuperheating region was given as:

$$U_{ds} = \frac{1}{\frac{1}{\eta_f A_{T,ds}}\left(\frac{1}{h^*_{ds,o}} + \frac{1}{h^*_{o,f}}\right) + \frac{d_o}{2\kappa_t} ln\left(\frac{d_o}{d_i}\right) + \frac{1}{A_{t,ds}}\left(\frac{1}{h^*_{ds,i}} + \frac{1}{h^*_{i,f}}\right)} \quad (10)$$

Where A_T is the total heat transfer area in the desuperheating section which is built by the total fin's surface area (A_f) plus the tube's total free surface area (A_t). For the case of the shell and tube with bare tubes the terms A_T and η_f were removed from Equation (10). The fin's efficiency is given by η_f, and κ_t is the thermal conductivity of the tube. The internal and external tube's diameters are represented by d_i and d_o respectively. The fouling convective factors are represented by $h^*_{i,f}$ and $h^*_{o,f}$ – inside and outside of the tube – with a value of 5 kW/m²·K per Sinnott [68]. The variables $h^*_{ds,i}$ and $h^*_{ds,o}$ are the convective heat transfer coefficients for the inside and outside of the tube respectively and can be found in the references given in Table 4.

Table 4: Overview of used references for designing the WHRS condenser unit.

Condenser Unit Section	Phenomena	Shell and Tube	Finned Tube
Coolant	Heat Transfer	Sinnott [68]	Wang et al. [70]
	Fin Efficiency	-	Schmidt [71]
	Friction	Sinnott [68]	Wang et al. [70]
Working Fluid	Heat Transfer	Sinnott [68], Gnielinski [72]	Shah [73], Gnielinski [72]
	Friction	Sinnott [68]	Petukhov [74], Müller-Steinhagen and Heck [75]
Condenser Unit	Temperature Correction Factor	Fakheri [76]	Shah and Sekulic [69]

Referring to Figure 9, the power required to move the cooling fluid through the condenser unit ($\dot{W}_S$) can be calculated as follows:

$$\dot{W}_S = \dot{m}_S(h_{S,i} - h_0) \quad (11)$$

Where h_0 is the specific enthalpy at the ambient conditions of the cooling fluid and $h_{S,i}$ is the specific enthalpy after the cooling fluid has passed through the fan or pump. To find the latter specific enthalpy, the same approach as the one described in equation (2) but using the isentropic efficiency for the air condenser unit fan (η_S). The mass flow rate for the cooling fluid ($\dot{m}_S$) was as follows:

$$\dot{m}_S = \frac{\dot{Q}_{co}}{(h_{S,o} - h_{S,i})} \quad (12)$$

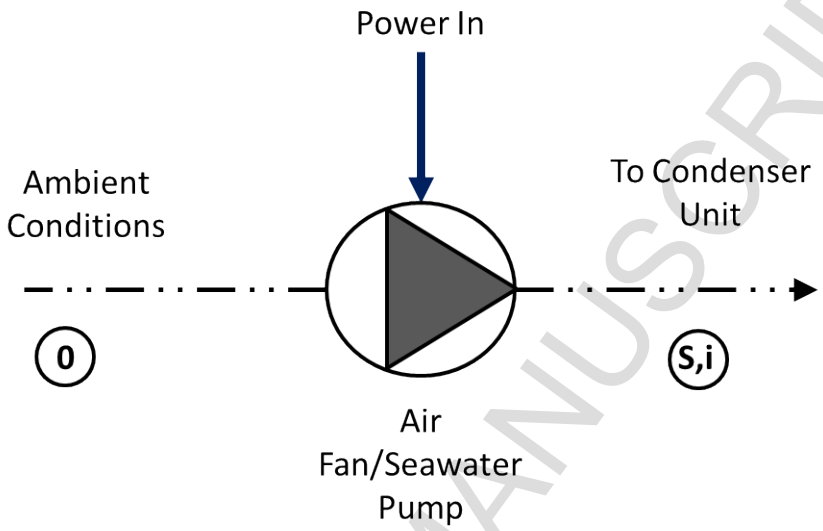

Figure 9: Schematic of condenser unit air fan or seawater pump.

A more detailed description of the equations used for the condenser units with their physical characteristics described can be found in Appendix A.

The net power output from the ORC unit ($\dot{W}_{WHRS}$) using the available waste heat from the scavenge air at a particular operating condition was given by the next expression:

$$\dot{W}_{WHRS} = \dot{W}_{ex} - \dot{W}_p - \dot{W}_S \quad (13)$$

3.1.2 OFF-DESIGN OPERATION

As the ship navigates along its route during the year, there will be instances when it will operate at off-design conditions. The seawater pump power change was related to the increase/decrease of the condenser unit duty but also to the seawater temperature over the months. In order to cope with these changes the seawater pump adapted its mass flow rate which affects its efficiency as given by Veres [77]. For the *U* values of both type of condenser units, the following expressions were used [78]:

$$U_{ds,off} = U_{ds,d} M^{0.6} \quad (14)$$

$$U_{co,off} = U_{co,d} M^{0.6} \quad (15)$$

Where *M* is the working fluid's mass flow rate ratio between the off-design and design condition. This same ratio was applied to the other WHRS heat exchangers.

3.2 SHIP PERFORMANCE

3.2.1 CARBON DIOXIDE REDUCTION

The benefit of using a WHRS on board can be measured in terms reduction in CO_2 emissions, (CS), given in tonnes per hour from the main engine by its reduction in load. Carbon dioxide emissions are directly proportional to the fuel burn. The annual fuel savings (FS_{annual}) achieved by reducing the main engine load was given by:

$$FS_{annual} = \frac{MT \sum_{i=0}^{OS} \sum_{j=0}^{OM} \dot{W}_{WHRS}(i,j) * SFOC_{me}(i,j) * t(i)}{10^6} \quad (16)$$

Where *MT* refers to the monthly single trips done by the containership, *OS* are the number of operating speeds as shown in Figure 4 and *OM* is the number of months. The time, in hours, spent at each operating speed is represented by *t* while $SFOC_{me}$ refers to the main engine's fuel consumption in g/kWh. The relationship between fuel burn and CO_2 emissions was given by:

$$CS_{annual} = FS_{annual} * C_F \quad (17)$$

Where C_F is the carbon conversion factor set at 3.1144 t CO_2 per t HFO [40]. The annual CO_2 savings were found by integrating the hourly carbon savings of each route segment in the year.

3.2.2 ENERGY EFFICIENCY DESIGN INDEX

The energy efficiency design index (EEDI) at the design condition can be found as follows:

$$\text{EEDI} = \frac{10^6 (CE - CS)}{F_i F_j TW} \quad (18)$$

Where *CE* represents the main engine carbon emissions which can be found using equations (16) and (17) but using the main engine power output instead of the WHRS. The transport work is represented by *TW* in deadweight tonnage per nautical mile, F_i and F_j are correction factors for capacity and power respectively taken from the guidelines for the calculation of the EEDI for new ships [40]. The 10^6 factor was used to correct the units from tonne to gram required by the EEDI formula. The EEDI for a ship is measured at 75% MCR of the main engine at the design condition, after the ship completes the certification procedure its EEDI value is effectively fixed for its entire life.

3.3 OPTIMISATION

The detailed designs of both the WHRS and condenser unit require a large number of variables to be explored with the aim of minimising the ship's annual CO_2 emissions. This very large dimensional search space requires an efficient optimisation approach which can return reliable data. The

optimisation approach used is a two-step single objective: Particle Swarm Optimisation (PSWO) followed by Pattern Search Optimisation (PSO).

Kennedy and Eberhart [79] developed PSWO to describe the movements of a bird inside a flock. The PSWO begins with a random distributed population or particles – data points as the ones shown in Table 5 – and looks for the optimum result of each iteration by using gradients or derivatives. Pattern search optimisation is a simple derivative-free heuristic method which has the task of finding new directions in the search space to improve the objective. The PSO starts with a reference point in the search space and depends on two different move methods to look for a better objective: Exploratory and Pattern. In the Exploratory move, the optimisation searches for an improving direction by creating nodes at fixed distance from the reference point and evaluating the function on those new nodes. Pattern has the task of improving the search time by increasing the distance to the reference point in the successful direction of the Exploratory move.

Table 5: Condenser unit design characteristics with their respective range of values for usage in northern waters.

Parameter	Cooling Fluid	Value/Characteristic	Variable selection
Material	Air	Aluminium	Fixed
	SW	Stainless Steel	Fixed
Flow	Air	Cross	Fixed
	SW	Counter	Fixed
Fan/pump Design Isentropic Efficiency (%)	Air	60	Fixed
	SW	80	Fixed
Tube Internal Diameter (mm)	Air/SW	16 – 100	Optimisation
Tube length (m)	Air/SW	1.83 – 7.32	Optimisation
Transversal Tube Pitch (mm)	Air	83	Fixed
	SW	1.4 * d_o	Fixed
Tube Layout	Air/SW	Rotated square	Fixed
Fin Height (mm)	Air	2 – 16	Optimisation
Fin Thickness (mm)	Air	$8x10^{-2}$ – 25 $x10^{-2}$	Optimisation
Fin Pitch (mm)	Air	2 – 24	Optimisation
Baffle Spacing (% of Shell Diameter)	SW	50 – 200	Optimisation
Inside and Outside Fouling Convective Factor ($kW/m^2 \cdot K$)	Air/SW	5	Fixed

Checks are added to the code which will verify that the solution is following the physical phenomena happening in a thermodynamic cycle (see Figure 10), for example acceptable pressure drop level inside the condenser unit. The optimisation process was run 240 times – 30 times per working and

cooling fluid combination – in order to have a wide range of different optimal WHRS designs which could explain how the operating conditions had an effect on the WHRS design and operation. Due to the large optimisation search space and the uniqueness of WHRS designs, a statistical analysis of the WHRS performance was done using a one-way analysis of variance (ANOVA). This model is suitable to analyse the mean difference – in this case the WHRS power output – between multiple groups at the same time.

Figure 10: Code structure developed for the analysis of marine WHRS in cold weathers. Inside the optimisation is found the design of the WHRS and condenser unit integrated to the speed profile and ship's route. This process happens for each working and cooling fluid and it tests the design over a year of operation.

3.4 Model validation

The model developed here is unique in different aspects such as the coupled optimisation process, the number of optimisation variables, the detailed WHRS condenser unit analysis and the ship's route integrated with the speed profile. This uniqueness makes it difficult to compare it to other works. The WHRS thermodynamic model and seawater condenser unit were used in Larsen et al. [45], Pierobon et al. [65] and Pierobon and Haglind [80]. In these works it was found that there was a 1% difference on the heat exchanger overall heat transfer coefficient when compared with a case outlined in Richardson and Peacock [81]. The air condenser unit model was compared to the example found in Gnielinski [82] for cross-flow heat exchangers. The outlet temperature from the heated fluid and the logarithmic temperature difference calculated by the model gave a deviation of 0.5% and 0.3%, respectively.

4. Results and discussion

4.1 Waste Heat Recovery System performance behaviour

In this first result section the aim is to understand the effects of working and cooling fluids and ship speed on the different marine WHRS designs and their condenser units. In order to observe the effects of working and cooling fluids and ship speed on the WHRS performance some of the operative conditions need to be fixed. The analysis is split into three parts:

1) effect of working and coolant fluids combinations on WHRS performance – power output and input – while holding the ambient temperature at 5.4°C – average temperature for air in June and also for seawater in April – and the ship speed at 23.3 knots;

2) WHRS performance change due to the speed profile given in Figure 4 for a single working fluid, both cooling fluids at ambient temperature of 5.4°C ; and

3) the condenser unit's bottom section – includes the fan/pump power consumption, heat rejection and physical characteristics – for a single working fluid, both cooling fluids at ambient temperature of 5.4°C and the ship speed at 23.3 knots.

Section 4.2 explores the effect that the ORC WHRS has on the EEDI of the container ship. In section 4.3, the integrated operative profile will be used to calculate the annual CO_2 emissions savings.

4.1.1 WORKING AND COOLING FLUID EFFECTS

The first step in the analysis compared the power output at design speed per working and cooling fluid. The simulations yielded 240 different WHRS – 30 each per working and cooling fluid combination. The ANOVA analysis was done grouping the ORC designs by working fluid and by cooling fluid in order to understand if there is a significant difference by groups.

The only statistically significant difference at the 95% confidence level – probability value[4] (p-value) lower than 0.05 – in the average power output at design speed when grouping by working fluids was found between WHRS using R236fa and WHRS using R1233zd(E) (see Table 6). Thus, the ORC using R236fa as working fluid performs differently than when using R1233zd(E), but when the analysis includes the other two working fluids there is not a significant difference between working fluids.

Table 6: Average power output and its standard deviation at the container ship design speed when grouping per working fluid. The table also shows the probability values (p-values) obtained using an analysis of variance (ANOVA).

Working Fluid	Power Output Average (kW)	Power Output Standard Deviation (kW)	p-value			
			R1233zd(E)	R245fa	R236fa	R236ea
R1233zd(E)	602	112		0.152	0.001	0.189
R245fa	641	83	0.152		0.499	1.000
R236fa	673	91	0.001	0.499		0.414
R236ea	640	105	0.189	1.000	0.414	

The statistical results can be seen more graphically in Figure 11, where it can be seen that there is no clear difference between populations of working fluids in either power output or power input. For the air case and looking at the power output, there is an overlap between 500 kW and 600 kW where it is possible to find both WHRS using R236fa and R1233zd(E), while for the case of seawater cooling the overlap happens between 650 kW and 770 kW. When looking only into the power input there is no clear difference between the working fluids. For air, the spread of power input for each working fluid is large at around 118.1 kW, while for seawater-cooled designs the spread is small with a maximum of 9.7 kW seen for R1233zd(E).

[4] It is the smallest significance level at which the null hypothesis can be rejected. In the case of ANOVA the null hypothesis is that the mean is the same for all groups.

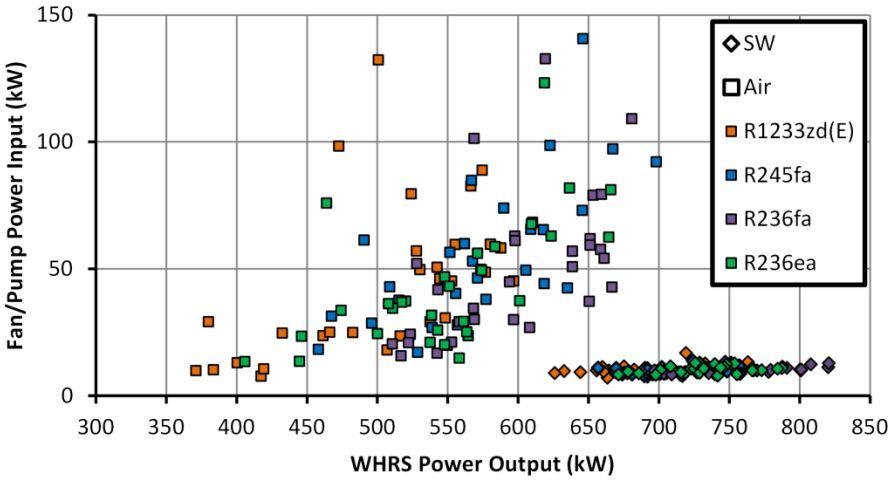

Figure 11: Air's fan and seawater's pump power input versus the power returned by the WHRS when the ship navigates at design speed.

When the power output is analysed by cooling fluid using a t-test[5] with assumed equal variances [83], important differences between seawater and air cooled plant are observed. The seawater cases have a significantly larger mean power output at 722 kW with a standard deviation of 40 kW compared to air at 556 kW with a standard deviation of 69 kW.

The power variation due to cooling fluid can be explained due to the power cost of cooling the WHRS. The highest WHRS power output using R236fa and seawater comes at 820 kW while for air it is 680 kW. The power difference is due to a higher waste heat absorption and pressure before entering the expander when using seawater as coolant which is controlled by the power cost of moving the coolant through the condenser unit. For the WHRS using seawater coolant the power input required for the WHRS excess heat is about 10% of the power required when cooling by air (i.e. 12 kW compared to 110 kW). The difference in power output due to working fluids is caused by the change in enthalpy at the expander and the amount of waste heat absorbed. In the case of the working fluid R1233zd(E) its largest enthalpy drop is 38.5 kJ/kg while for the working fluid R236fa is 30.1 kJ/kg, caused mainly due to a lower pressure after expansion for the former working fluid. Interestingly, R236fa achieves a larger power output than a WHRS using R1233zd(E) due to its larger heat absorption. This causes larger mass flow rates, 18.3 kg/s when using R236fa as working fluid and 14.7 kg/s when using R1233zd(E).

In Figure 12 it can be seen that the choice of working fluid has much less impact on performance than the choice of cooling fluid. In order to reduce the search space and to focus on a more detailed comparison of the two cooling fluids a single representative working fluid was utilised for the remainder of the analysis. Hydrochlorofluoroolefin (R1233zd(E)) was selected as it has a significantly lower global warming potential (GWP_{100}) than the alternatives (see Table 2) even though it does not offer the greatest power output of the four candidates.

[5] A t-test is suitable for binary mean comparisons of small groups of data.

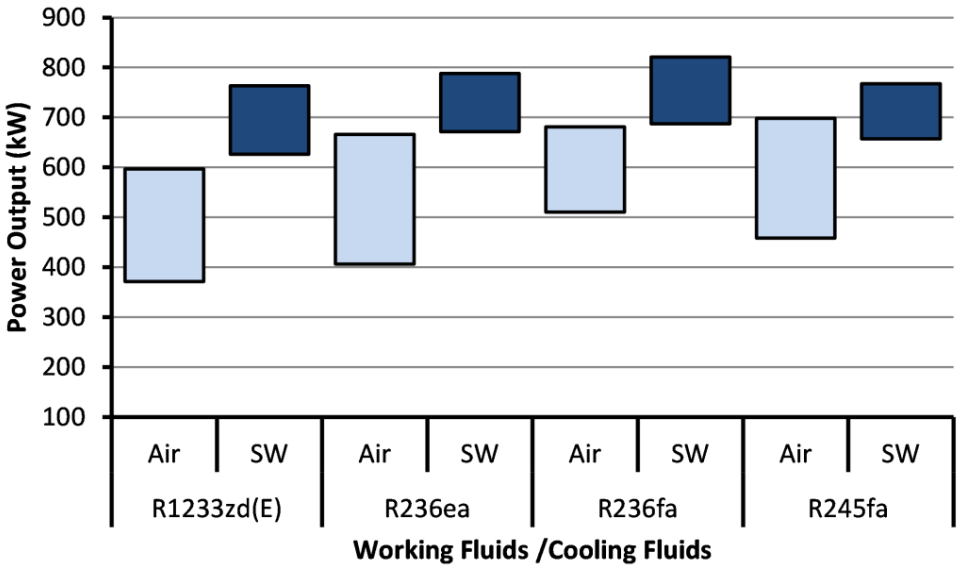

Figure 12: Power output for different ORC WHRS cooled by seawater or air at the ship's design speed.

4.1.2 Waste Heat Recovery System power production at different speeds

The maximum power output achieved by the R1233zd(E) WHRS is when it is cooled by seawater and the ship's speed is between 100% and 105% of the design speed (see Figure 13) due to a higher waste heat temperature and availability – up to 14,340 kW [39] – which enhances the waste heat absorption by the ORC. Below these speeds, air-cooled WHRS have designs that match or achieve larger power outputs. At the lower end of the speed spectrum only the air-cooled designs can operate, however the useful power produced is low.

The ship operating profile is another important factor for annual CO_2 reduction. For example, at the 105% of the design speed the WHRS' largest power output for both cooling fluids is achieved. But this condition only represents 4% of the time the ship is operating. From Figure 4, the ship will spend most of its time between 85% and 100% of its design speed and at these speeds there is a considerable power return which will be critical for CO_2 reductions. Below 85% of the design speed, some WHRS designs can operate but their power output is low, indicating that it would be better to switch-off the WHRS and use the available waste heat to support heating on board.

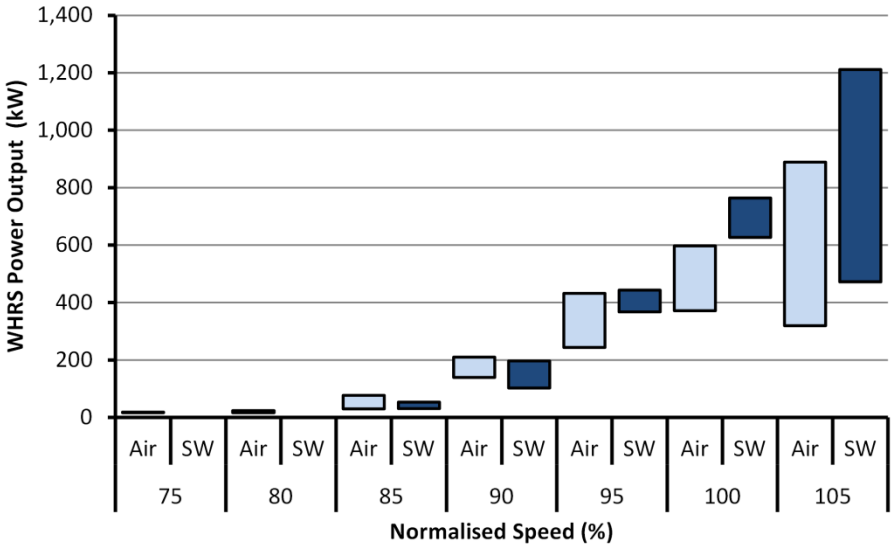

Figure 13: Maximum and minimum power produced by each R1233zd(E) WHRS not considering the condenser unit's power requirement, grouped by cooling fluid at different ship's speeds.

4.1.3 CONDENSER UNIT PERFORMANCE

As the ship navigates in northern waters, different engine loadings are requested which will determine the WHRS performance but also the condenser unit's heat rejection load. The heat output and the cooling fluid enthalpy change across the condenser unit dictate the cooling fluid mass flow rate. The minimum mass flow rate at design speed for the air-cooled case was 152 kg/s while the maximum for the seawater case was 128 kg/s. For air-cooled designs the heat rejection at the condenser section at design speed goes from 2,320 kW to 4,705 kW; for seawater-cooled designs the range moves between 4,409 kW and 6,442 kW. While the increase in heat load at the condenser unit explains the increment in mass flow rate for each cooling fluid, it does not explain the difference in mass flow rates within the cooling fluids. Air-cooled systems have an enthalpy change between the fan's exit and the condenser unit's pinch point between 7.3 kJ/kg and 14.5 kJ/kg, while for seawater this goes from 44.4 kJ/kg to 61.2 kJ/kg. The difference is due to air's lower heat capacity which produces a faster temperature rise. This limits the heat absorption and requires larger mass flow rates to cover the heat rejection demand.

The construction of the condenser unit will determine the other part of the fan/pump power requirement. Starting with the heat transfer area, air-cooled designs ranged from 5,238 m^2 to 19,098 m^2 while for the seawater case, it is from 823 m^2 to 2,207 m^2. This difference has to do with the cooling fluid's overall heat transfer coefficient (U). Seawater-cooled WHRS had an U_{ds} that fell between 49.3 $W/m^{2}\cdot°C$ and 66.2 $W/m^{2}\cdot°C$, while U_{co} was between 357.0 $W/m^{2}\cdot°C$ and 640.7 $W/m^{2}\cdot°C$. For the air-cooled case, U_{ds} went from 4.7 $W/m^{2}\cdot°C$ to 19.1 $W/m^{2}\cdot°C$, and U_{co} from 15.1 $W/m^{2}\cdot°C$ to 44.6 $W/m^{2}\cdot°C$.

The smaller mass flow rates using seawater, plus a lesser heat transfer area requirement produce smaller condenser unit designs – volume could be found from 6.2 m^3 to 19.3 m^3. When cooling with air, the volume went from 35.1 m^3 to the maximum volume allowed of 38.5 m^3. These are practical values for a large container ship.

Air's lower density and viscosity, when compared to seawater, results in condenser units which tend to have a much lower pressure drop than in the case of seawater (see Figure 14). So, even though air condenser units have generally smaller pressure drops, it is the air condenser unit's large frontal area plus a high mass flow rate that gives a high energetic cost to the pressure change at the fan (see Equation (A.7)) and hence a high power input (see Figure 14). Air-cooled WHRS exhibit the most extreme cases of power requirement with a maximum of 132 kW while for seawater-cooled designs is 17 kW.

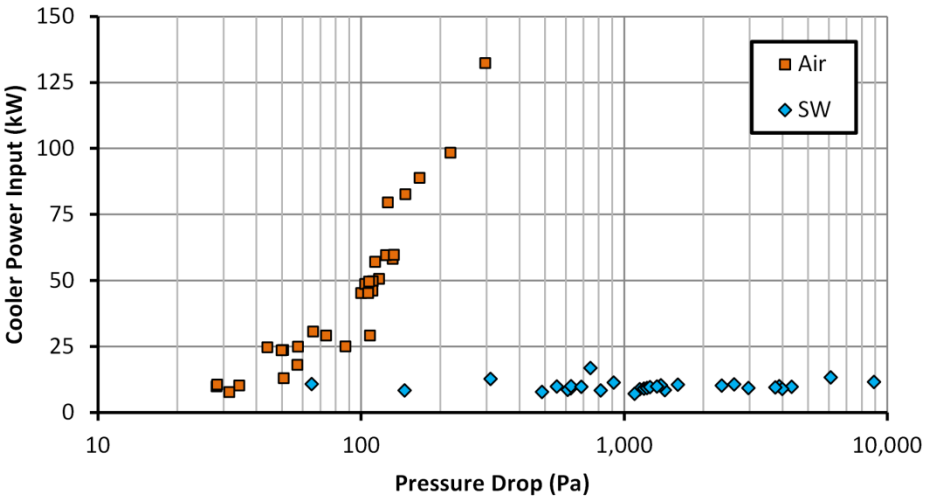

Figure 14: Fan and pump power input demanded at the design speed and a temperature of 5.4˚C.

4.2 Impact on the Energy Efficiency Design Index

This section analyses how installing an ORC WHRS, depending on its working and cooling fluid, at the container ship's design stage could result in a reduced (better) EEDI. The ship's EEDI at design point when installing an ORC is measured at an ambient temperature where both cooling fluids have a temperature of 5.4˚C and compared to the base line value of 17.647 g CO_2/t-nm with no ORC WHRS installed (see Figure 15).

The ORC designs cooled by seawater achieve the lowest EEDI at 17.336 g CO_2/t-nm – a reduction of around 2.3% from the baseline value while the best air-cooled design achieves an EEDI of 17.446 g CO_2/t-nm. Livanos et al. [84] found that a ferry using HFO could reduce its EEDI by around 4.6% when using a water-based RC extracting the waste heat from the exhaust gas. Theotokatos and Livanos [85] found that a WHRS could reduce a bulk carrier EEDI from 5.11 g CO_2/t-nm to 5.02 g CO_2/t-nm, a reduction of around 1.8%. While the type of ship, engine power, operating

conditions and WHRS designs are different in each study, the comparison suggests that the findings of the present study are similar to those of previous works.

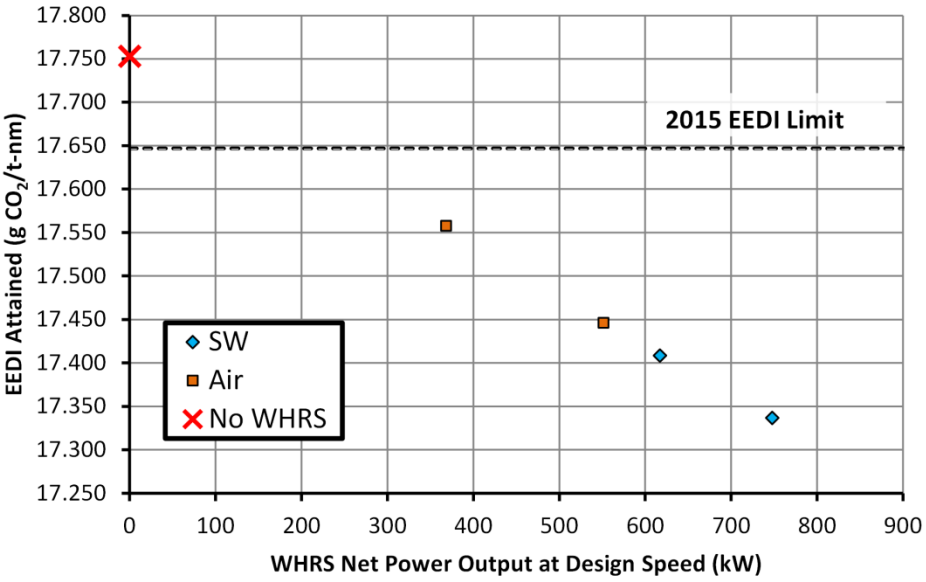

Figure 15: Different EEDI achieved when the ship is designed with a marine R1233zd(E) WHRS using the waste heat available from the container ship scavenge air system. It only shows the minimum (best) and maximum EEDI obtained with different cooling fluids. The figure also shows the 2015 EEDI limit for a container ship and the EEDI achieved without any mitigating green technology installed on board.

Under the current marine fuel price and regulations, achieving EEDI compliance could be one of the most common scenarios for a ship owner. Air-cooled designs show smaller reductions in the EEDI but following from the discussion at the end of the previous section, an air-cooled WHRS could be a more affordable option for the studied container ship to comply with the EEDI limit established.

4.3 Annual CO_2 emission reductions

The analysis thus far has considered a single ambient temperature of 5.4°C for the ambient cooling fluids and a constant ship speed of 23.3 knots. To obtain the annual CO_2 emissions the variation of cold sink temperature over the year must be considered (see Figures Figure 2 and Figure 3) and the operating profile of the ship, (see Figure 4). Figure 16 shows the average net power output change by month using January as the datum; a ship speed of 23.3 knots is used. It is clear that the air-cooled design is more sensitive to ambient temperature changes than the water-cooled design even when it is taken into account that sea temperature only varies by 5°C over a year and ambient air by 9°C.

At any given ship speed, due to the WHRS having a fixed saturated temperature after expansion (T_3), the changes in the net power production during the year are caused solely by the fan/pump power input which changes due to variation in the monthly temperature (see Figure 16).

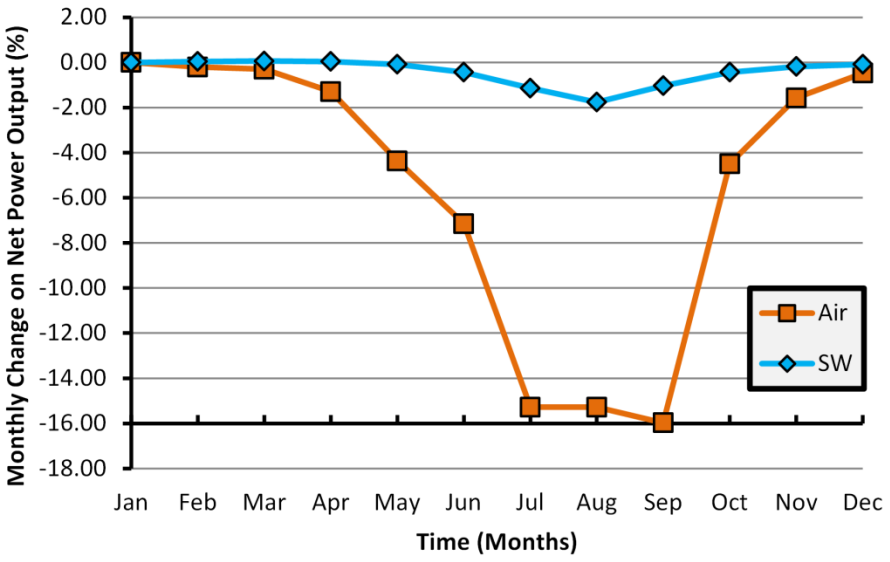

Figure 16: Average net power output change during a year for the R1233zd(E) WHRS designs when compared to the WHRS January average net power output at a speed of 23.3 knots.

The air/seawater temperature increase causes a reduction in the cooling fluids' enthalpy change between the fan/pump exit and the condenser unit's pinch point, requiring larger mass flow rates to be able to reject the excess heat. In the case of air, the average fan power requirement goes from 12.0 kW in January (minimum power requirement) to 90.6 kW in September (maximum power requirement), an increment of 655%. In the case of seawater, the minimum power input from the seawater pump is in March at 10.2 kW, and the maximum in August at 22.7 kW which represents a change of 123%. Habl et al. [28] reported a drop of 5% in the net power generated from winter months to summer months in a power plant located in the south of Spain and cooled with air; this was due to an increase in fan power consumption of around 120% in the same period (i.e. from 1,250 kW to 2,750 kW).

As expected the monthly CO_2 savings (see Figure 17) follow the behaviour seen for the monthly net power output change and the inclusion of the operating profile has little impact as the ship spends the majority of its time either near its design speed or in port when the WHRS is not in use. On average, the R1233zd(E) WHRS when cooled by seawater can reduce CO_2 by 599 t annually while when cooled by air the annual reductions of CO_2 are 471 t.

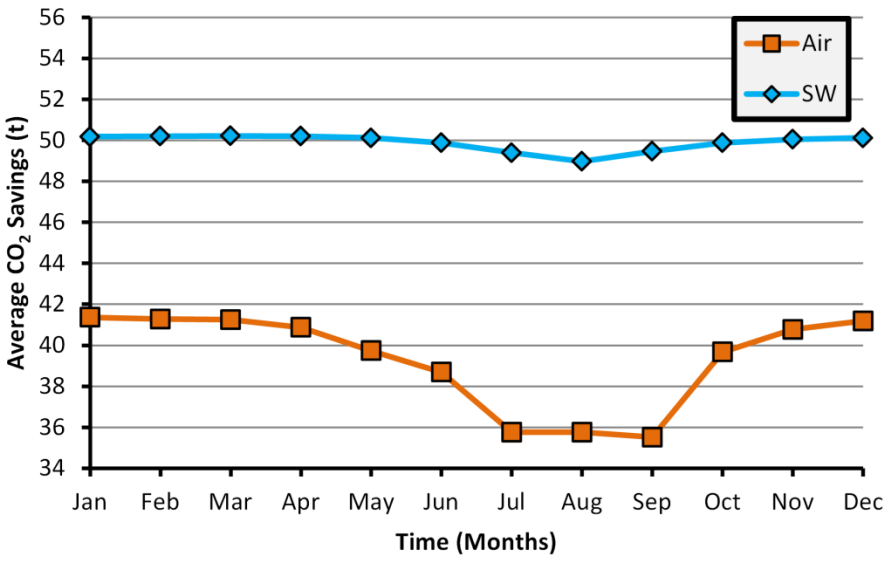

Figure 17: Average monthly CO_2 emission savings due to the monthly ambient temperature change in air and seawater during the year on the route studied when R1233zd(E) is used as working fluid.

CONCLUSIONS

In this paper the performance of a marine ORC-based WHRS using air or seawater as cooling fluids and a selection of four working fluids were studied with the aim of taking advantage of the low air temperatures found above the Arctic Circle. This work calculated the power output of the WHRS, condenser characteristics, EEDI and annual CO_2 emission reductions when using the scavenge air waste heat coming from the engine of a 4,100 TEU container ship navigating in the Arctic waters.

A two-stage single objective approach was used for this work with the aim of finding within a very large variable space the most optimal WHRS under the ship's operating conditions. The optimisation approach was run for 240 times in order have a strong sample of optimum designs. From the different WHRS designs it was possible to distinguish that the four working fluids selected presented similar results with a much greater variation being demonstrated between the two cooling fluids. This presented an opportunity to significantly reduce the variable space by using a single working fluid for subsequent analysis. Hydrochlorofluoroolefin (R1233zd(E)) was selected, although not offering the greatest power output it has a significantly lower global warming potential than the three other candidates.

The results suggest that despite the ambient air temperature always being below the seawater temperature the more suitable cooling fluid is seawater. Air's low specific heat capacity requires large flow rates of the coolant and heat transfer area to absorb the excess heat from the marine WHRS. This produces large condenser units (not necessarily an issue on a container ship) and high fan power requirement – a maximum of 132 kW. On the other hand, seawater designs had more compact condensers and a much lower maximum pump power requirement of 17 kW but have to interface with seawater which is corrosive. The optimisation process due to the high power input for air-condenser

units select ORC systems that absorb less waste heat from the scavenge air and hence have a lower installed power – 546 kW compared to 847 kW from the seawater-cooled WHRS.

In general, the high power output of seawater-cooled WHRS coupled with low seawater pump power consumption achieve the largest CO_2 emission reduction over the course of a year with an average saving of about 599 t while air-cooled ORC reduce the ship's CO_2 of about 471 t. The air-cooled WHRS is more sensitive to changes in ambient temperature than the seawater-cooled plant. On environmental regulations, all of the seawater-cooled and air-cooled WHRS achieve EEDI compliance for the 4,100 TEU container ship – under the 2015 EEDI maximum limit of 17.647 g CO_2/t-nm – but the seawater-cooled designs achieved the lowest EEDI at 17.336 g CO_2/t-nm.

The results indicate that the benefits of air's lower temperature compared to seawater in the southern regions of the Arctic are overshadowed by the air condenser unit power demands and sizing. However, air-cooling may offer a lower maintenance and cheaper systems as it avoids contact with corrosive seawater. It could become more attractive for ships operating in high latitudes with colder air temperatures.

ACKNOWLEDGEMENTS

This work was supported by the Mexican National Council of Science and Technology (CONACYT) [grant number 213748]; the Institute of Marine Engineering, Science & Technology under the Stanley Gray Award; and the Department of Mechanical Engineering and Graduate School at UCL [grant number 2.13/14.RP.BEM].

REFERENCES

[1] National Snow And Ice Data Center. Sea Ice Index 2013:1. http://nsidc.org/data/seaice_index/ (accessed December 12, 2013).

[2] Smith LC, Stephenson SR. New Trans-Arctic shipping routes navigable by midcentury. Proc Natl Acad Sci U S A 2013;110:E1191-5. doi:10.1073/pnas.1214212110.

[3] Winther M, Christensen JH, Plejdrup MS, Ravn ES, Eriksson ÓF, Kristensen HO. Emission inventories for ships in the arctic based on satellite sampled AIS data. Atmos Environ 2014;91:1–14. doi:10.1016/j.atmosenv.2014.03.006.

[4] Corbett JJ, Lack DA, Winebrake JJ, Harder S, Silberman JA, Gold M. Arctic shipping emissions inventories and future scenarios. Atmos Chem Phys 2010;10:9689–704. doi:10.5194/acp-10-9689-2010.

[5] Rodrigue J-P. The Geography of Transport Systems 2013:1. http://people.hofstra.edu/geotrans/eng/ch1en/conc1en/polarroutes.html (accessed December 12, 2013).

[6] Smith TW., Traut M, Bows-Larkin A, K. A, McGlade C, Wrobel P. CO2 Targets, Trajectories and Trends for International Shipping. Manchester: 2015.

[7] Lloyd's Register. Provisional Rules for the Winterisation of Ships 2012 2012:104.

[8] MAN Diesel & Turbo. Influence of Ambient Temperature Conditions 2014:17.

[9] Suárez de la Fuente S. Reducing Shipping Carbon Emissions under Real Operative Conditions: A Study of Alternative Marine Waste Heat Recovery Systems based on the Organic Rankine Cycle. UCL, 2016.

[10] Schmid H. Waste Heat Recovery (WHR): Fuel Savings With Less Emissions. Green Sh. Technol. Conf., London: 2004, p. 10.

[11] Balaji R, Yaakob O. An analysis of shipboard waste heat availability for ballast water treatment. J Mar Eng Technol 2012;11:15–29.

[12] Shu G, Liang Y, Wei H, Tian H, Zhao J, Liu L. A review of waste heat recovery on two-stroke IC engine aboard ships. Renew Sustain Energy Rev 2013;19:385–401. doi:10.1016/j.rser.2012.11.034.

[13] Vanslambrouck B, Vankeirsbilck I, Gusev S, Paepe M De. Efficiency comparison between the steam cycle and the organic Rankine cycle for small scale power generation. Renew. Energy World Conf. Expo North Am., vol. 32, Long Beach: Howeast, Universiteit Gent,; 2012, p. 13.

[14] Yamamoto T, Furuhata T, Arai N, Mori K. Design and testing of the Organic Rankine Cycle. Energy 2001;26:239–51. doi:10.1016/S0360-5442(00)00063-3.

[15] Kalikatzarakis M, Frangopoulos CA. Multi-criteria selection and thermo-economic optimization of Organic Rankine Cycle system for a marine application. In: Zevenhoven R, editor. Int. Conf. Effic. Cost, Optim. Simul. Environ. Impact Energy Syst., Turku: Abo Akademi University; 2014, p. 15.

[16] Soffiato M, Frangopoulos CA, Manente G, Rech S, Lazzaretto A. Design optimization of ORC systems for waste heat recovery on board a LNG carrier. Energy Convers Manag 2015;92:523–34. doi:10.1016/j.enconman.2014.12.085.

[17] Cengel YA, Boles MA. Thermodynamics: An Engineering Approach. 6th ed. Singapore: McGraw-Hill; 2007.

[18] Stanzel N, Streule T, Preißinger M, Brüggemann D. Comparison of Cooling System Designs for an Exhaust Heat Recovery System Using an Organic Rankine Cycle on a Heavy Duty Truck. Energies 2016;9:928. doi:10.3390/en9110928.

[19] Rayner NA, Brohan P, Parker DE, Folland CK, Kennedy JJ, Vanicek M, et al. Improved analyses of changes and uncertainties in sea surface temperature measured in situ since the mid-nineteenth century: the HadSST2 data set. J Clim 2006;19:446–69.

doi:10.1175/JCLI3637.1.

[20] Jones PD, Lister DH, Osborn TJ, Harpham C, Salmon M, Morice CP. Hemispheric and large-scale land-surface air temperature variations: An extensive revision and an update to 2010. J Geophys Res 2012;117:D05127. doi:10.1029/2011JD017139.

[21] Jones PD, New M, Parker DE, Martin S, Rigor IG. Surface air temperature and its changes over the past 150 years. Rev Geophys 1999;37:173. doi:10.1029/1999RG900002.

[22] Moore J, Grimes R, Walsh E, O'Donovan A. Modelling the thermodynamic performance of a concentrated solar power plant with a novel modular air-cooled condenser. Energy 2014;69:378–91. doi:10.1016/j.energy.2014.03.028.

[23] Salimpour MR, Bahrami Z. Thermodynamic analysis and optimization of air-cooled heat exchangers. Heat Mass Transf 2010;47:35–44. doi:10.1007/s00231-010-0672-9.

[24] Cristiani P, Giancola U. Prevention of fouling and microbial Corrosion in Power Stations using Seawater as a Coolant. In: Müller-Steinhagen H, editor. Heat Exch. Fouling Mitig. Clean. Technol. 1st ed., Essen: Publico Publications; 2000, p. 334–49.

[25] British Standard Institution. BS 6349-1:2000 Maritime Structures - Part 1: Code of Practice for General Criteria 2002:202.

[26] Bustamante JG, Rattner AS, Garimella S. Achieving near-water-cooled power plant performance with air-cooled condensers. Appl Therm Eng 2016;105:362–71. doi:10.1016/j.applthermaleng.2015.05.065.

[27] Zhai H, Rubin ES. Performance and cost of wet and dry cooling systems for pulverized coal power plants with and without carbon capture and storage. Energy Policy 2010;38:5653–60. doi:10.1016/j.enpol.2010.05.013.

[28] Habl P, Blanco-Marigorta AM, Erlach B. Exergoeconomic comparison of wet and dry cooling technologies for the Rankine cycle of a solar thermal power plant. In: Desideri U, Manfrida G, Sciubba E, editors. Effic. Cost, Optim. Simul. Environ. Impact Energy Syst., Perugia: Firenze University Press; 2012, p. 300.1-300.14.

[29] He S, Gurgenci H, Guan Z, Hooman K, Zou Z, Sun F. Comparative study on the performance of natural draft dry, pre-cooled and wet cooling towers. Appl Therm Eng 2016;99:103–13. doi:10.1016/j.applthermaleng.2016.01.060.

[30] Usman M, Imran M, Yang Y, Lee DH, Park B-S. Thermo-economic comparison of air-cooled and cooling tower based Organic Rankine Cycle (ORC) with R245fa and R1233zde as candidate working fluids for different geographical climate conditions. Energy 2017;123:353–66. doi:10.1016/j.energy.2017.01.134.

[31] Google Maps. Iceland - Norway 2014:1. https://www.google.co.uk/maps/@65.6656819,-5.2133144,6.08z (accessed November 5, 2014).

[32] Containership-Info. JPO LIBRA 2014:1. http://www.containership-info.com/ (accessed September 22, 2014).

[33] Clarkson Research Services Limited. Shipping Intelligence Network 2013.

[34] Banks C, Turan O, Incecik A, Theotokatos G, Izkan S, Shewell C, et al. Understanding ship operating profiles with an aim to improve energy efficient ship operations. Low Carbon Shipp. Conf., London: 2013, p. 11.

[35] Holtrop J, Mennen GG. An Approximate Power Prediction Method. Int Shipbuild Prog 1982;29:166–70.

[36] Holtrop J. A statistical re-analysis of resistance and propulsion data. Int Shipbuild Prog 1984;31:272–6.

[37] Det Norske Veritas AS. DNV-OS-A201: Winterization for Cold Climate Operations (Tentative) 2013:83.

[38] Molland A. The maritime engineering reference book: a guide to ship design, construction and operation. 1st ed. Oxford: Butterworth-Heinemann; 2008.

[39] MAN Diesel & Turbo. Engine room and performance data for 8S90ME-C9.5-TII with high load tuning. 2015:10.

[40] International Maritime Organization. Resolution MEPC.212(63) - 2012 Guidelines On The Method Of Calculation Of The Attained Energy Efficiency Design Index (EEDI) For New Ships. 2012.

[41] The Baltic and International Maritime Council. Updated BIMCO EEDI Calculator. Products 2013. https://www.bimco.org/en/Products/EEDI.aspx (accessed October 15, 2014).

[42] Watson N, Janota MS. Turbocharging the Internal Combustion Engine. 1st ed. London: Macmillan Education UK; 1982. doi:10.1007/978-1-349-04024-7.

[43] Øien HA. Energy efficient operation of ships. Norwegian University of Science and Technology, 2011.

[44] Xiros N. Marine Engine Thermodynamics. Robust Control Diesel Sh. Propuls. 1st ed., Lodnon: Springer-Verlag London Ltd.; 2002, p. 13–42. doi:10.1007/978-1-4471-0191-8_2.

[45] Larsen U, Pierobon L, Haglind F, Gabrielii C. Design and optimisation of organic Rankine cycles for waste heat recovery in marine applications using the principles of natural selection. Energy 2013;55:803–12. doi:10.1016/j.energy.2013.03.021.

[46] Datla BV, Brasz J. Comparing R1233zd and R245fa for Low Temperature ORC Applications. Int. Refrig. Air Cond. Conf., Purdue: Purdue University; 2014, p. 7.

[47] Molés F, Navarro-Esbrí J, Peris B, Mota-Babiloni A, Barragán-Cervera Á, Kontomaris K (Kostas). Low GWP alternatives to HFC-245fa in Organic Rankine Cycles for low temperature heat recovery: HCFO-1233zd-E and HFO-1336mzz-Z. Appl Therm Eng 2014;71:204–12. doi:10.1016/j.applthermaleng.2014.06.055.

[48] Forster P, Ramaswamy V, Artaxo P, Berntsen T, Betts R, Fahey DW, et al. 2007: Changes in Atmospheric Constituents and in Radiative Forcing. In: Solomon S, Qin D, Manning M, Chen Z, Marquis M, Averyt KB, et al., editors. Clim. Chang. 2007 Phys. Sci. Basis. Contrib. Work. Gr. I to Fourth Assess. Rep. Intergov. Panel Clim. Chang. First, Cambridge: Cambridge University Press; 2007, p. 129–234.

[49] Hulse RJ, Basu RS, Singh RR, Thomas RHP. Physical Properties of HCFO-1233zd(E). J Chem Eng Data 2012;57:3581–6. doi:10.1021/je300776s.

[50] Myhre G, Shindell D, Bréon F-M, Collins W, Fuglestvedt J, Huang J, et al. 2013: Anthropogenic and Natural Radiative Forcing. In: Stocker TF., Qin D., Plattner G-K, Tignor M;, Allen SK., Boschung J., et al., editors. Clim. Chang. 2013 Phys. Sci. Basis. Contrib. Work. Gr. I to Fifth Assess. Rep. Intergov. Panel Clim. Chang. 1st ed., Cambridge and New York: Cambridge University Press; 2013, p. 659–740.

[51] Rusch G, Bingham P, Farrar D, Jepson G, Libre J-M, Malinverno G, et al. JACC 044 : 1,1,1,3,3-pentafluoropropane (HFC-245fa) (CAS No. 460-73-1). Brussels: 2004.

[52] Rui X, Pan J, Wang Y. An equation of state for the thermodynamic properties of 1,1,1,2,3,3-hexafluoropropane (R236ea). Fluid Phase Equilib 2013;341:78–85. doi:10.1016/j.fluid.2012.12.026.

[53] Calm JM, Hourahan GC. Refrigerant Data Summary. Eng Syst 2001:74–88.

[54] Honeywell. Genetron 245fa (pressurized), Material Safety Datasheet GTRN-0037. Morristown: 2001.

[55] Honeywell. Solstice ® 1233zd (E) Safety Data Sheet 2014:1–14.

[56] Kontomaris K. HFO-1336mzz-Z: High Temperature Chemical Stability and Use as A Working Fluid in Organic Rankine Cycles. Int. Refrig. Air Cond. Conf., Purdue: Purdue University; 2014, p. 10.

[57] Angelino G, Invernizzi C. Experimental investigation on the thermal stability of some new zero ODP refrigerants. Int J Refrig 2003;26:51–8. doi:10.1016/S0140-7007(02)00023-3.

[58] Airgas USA LLC. Safety Data Sheet HFC-236fa 2015:11.

[59] Lemmon EW, Huber ML, McLinden MO. NIST Reference Fluid Thermodynamic and Transport Properties Database 2010.

[60] International Maritime Organization. SOLAS, Consolidated Edition 2009. 5th ed. London: IMO Publishing; 2009.

[61] Mondejar ME, Cignitti S, Abildskov J, Woodley JM, Haglind F. Prediction of properties of new halogenated olefins using two group contribution approaches. Fluid Phase Equilib 2017;433:79–96. doi:10.1016/j.fluid.2016.10.020.

[62] International Maritime Organization. Draft International Code of Safety for Ships using Gases or other Low flashpoint Fuels (IGF Code) 2014.

[63] Det Norske Veritas AS. Tentative Rules for Low Flashpoint Liquid Fuelled Ship Installations 2013:37.

[64] Suárez de la Fuente S, Roberge D, Greig AR. Safety and CO2 emissions: Implications of using organic fluids in a ship's waste heat recovery system. Mar Policy 2017;75:191–203. doi:10.1016/j.marpol.2016.02.008.

[65] Pierobon L, Larsen U, Haglind F, Elmegaard B, Nguyen T-V. Multi-objective optimization of organic Rankine cycles for waste heat recovery: Application in an offshore platform. Energy 2013;58:538–49. doi:10.1016/j.energy.2013.05.039.

[66] Suárez de la Fuente S, Greig A. Making shipping greener: comparative study between organic fluids and water for Rankine cycle waste heat recovery. J Mar Eng Technol 2015;14:70–84. doi:10.1080/20464177.2015.1077601.

[67] Bell IH, Wronski J, Quoilin S, Lemort V. Pure and Pseudo-pure Fluid Thermophysical Property Evaluation and the Open-Source Thermophysical Property Library CoolProp. Ind Eng Chem Res 2014;53:2498–508. doi:10.1021/ie4033999.

[68] Sinnott RK. Heat-transfer Equipment. Coulson Richardson's Chem. Eng. Vol. 6 - Chem. Eng. Des. 4th ed., Oxford: Elsevier; 2005, p. 634–793.

[69] Shah RK, Sekulic DP. Fundamentals Of Heat Exchanger Design. 1st ed. New Jersey: John Wiley & Sons, Inc.; 2003.

[70] Wang C-C, Lee C-J, Chang C-T, Lin S-P. Heat transfer and friction correlation for compact louvered fin-and-tube heat exchangers. Int J Heat Mass Transf 1999;42:1945–56. doi:10.1016/S0017-9310(98)00302-0.

[71] Schmidt TE. Heat transfer calculations for extended surfaces. Refrig Eng 1949;4:351–7.

[72] Gnielinski V. New Equations for Heat and Mass Transfer in Turbulent Pipe and Channel Flow. Int J Chem Eng 1976;16:359–68.

[73] Shah MM. A general correlation for heat transfer during film condensation inside pipes. Int J Heat Mass Transf 1979;22:547–56. doi:10.1016/0017-9310(79)90058-9.

[74] Petukhov BS. Heat transfer and friction in turbulent pipe flow with variable physical properties. Adv Heat Transf 1970;6.

[75] Müller-Steinhagen H, Heck K. A simple friction pressure drop correlation for two-phase flow in pipes. Chem Eng Process Process Intensif 1986;20:297–308. doi:10.1016/0255-2701(86)80008-3.

[76] Fakheri A. A General Expression for the Determination of the Log Mean Temperature Correction Factor for Shell and Tube Heat Exchangers. J Heat Transfer 2003;125:527. doi:10.1115/1.1571078.

[77] Veres JP. Centrifugal and Axial Pump Design and Off-Design Performance Prediction. Cleveland: 1994.

[78] Incropera FP, Dewitt DP, Bergman TL, Lavine AS. Fundamentals of Heat and Mass Transfer. 6th ed. Hoboken: John Wiley & Sons, Inc.; 2007.

[79] Kennedy J, Eberhart R. Particle swarm optimization. Proc. ICNN'95 - Int. Conf. Neural

Networks, vol. 4, Perth: IEEE; 1995, p. 1942–8. doi:10.1109/ICNN.1995.488968.

[80] Pierobon L, Haglind F. Design and optimization of air bottoming cycles for waste heat recovery in off-shore platforms. Appl Energy 2014;118:156–65. doi:10.1016/j.apenergy.2013.12.026.

[81] Richardson JF, Peacock DG. Coulson and Richardson's Chemical Engineering Volume 3 - Chemical and Biochemical Reactors and Process Control. 3rd ed. Oxford: Elsevier; 1994.

[82] Gnielinski V. G7 Heat Transfer in Cross-flow Around Single Rows of Tubes and Through Tube Bundles. In: VDI-Gesellschaft Verfahrenstechnik und Chemieingenieurwesen, editor. VDI Heat Atlas. 2nd ed., Düsseldorf: Springer-Verlag Berlin Heidelberg; 2010, p. 725–30.

[83] Student. The Probable Error of a Mean. Biometrika 1908;6:1–25. doi:10.2307/2331554.

[84] Livanos GA, Theotokatos G, Pagonis D-N. Techno-economic investigation of alternative propulsion plants for Ferries and RoRo ships. Energy Convers Manag 2014;79:640–51. doi:10.1016/j.enconman.2013.12.050.

[85] Theotokatos G, Livanos G. Techno-economical analysis of single pressure exhaust gas waste heat recovery systems in marine propulsion plants. Proc Inst Mech Eng Part M J Eng Marit Environ 2012;227:83–97. doi:10.1177/1475090212457894.

[86] Shah MM. A general correlation for heat transfer during film condensation inside pipes. Int J Heat Mass Transf 1979;22:547–56. doi:10.1016/0017-9310(79)90058-9.

[87] Robinson KK, Briggs DE. Pressure drop of air flowing across triangular pitch banks of finned tubes. Chem Eng Prog Symp Ser 1966;62:177–84.

[88] Walraven D, Laenen B, D'haeseleer W. Minimizing the levelized cost of electricity production from low-temperature geothermal heat sources with ORCs: Water or air cooled? Appl Energy 2015;142:144–53. doi:10.1016/j.apenergy.2014.12.078.

[89] The MathWorks Inc. Find minimum of single-variable function on fixed interval - MATLAB fminbnd - MathWorks United Kingdom. Optimization 2015:1. http://uk.mathworks.com/help/matlab/ref/fminbnd.html?refresh=true (accessed April 27, 2015).

APPENDIX A

A.1 SHELL AND TUBE HEAT EXCHANGER

This section will describe the model for a shell and tube heat exchanger. To find the convective heat transfer coefficients for the inside of the tube ($h^*_{ds,i}$) the following equation was used [68]:

$$h^*_{ds,i} = F_{ht,i}\frac{\kappa_S}{d_i}Re_d Pr^{0.33}\left(\frac{\mu_t}{\mu_{t,w}}\right)^{0.14} \quad (A.1)$$

The variable μ_t is the dynamic viscosity at the average tube's temperature between the inlet and outlet, while $\mu_{t,w}$ is the dynamic viscosity at the wall temperature. The factor $F_{ht,i}$ represents the heat transfer correction factor from the tube side and was evaluated as shown in Sinnott [68]. The variable κ_S was used for the seawater's thermal conductivity, while Re_d and Pr are the Reynolds and Prandtl number inside the tubes respectively. From the shell side, the heat transfer coefficient ($h^*_{ds,o}$) was found with the following equation:

$$h^*_{ds,o} = F_{ht,o}\frac{\kappa_{wf}}{d_s}RePr^{0.33}\left(\frac{\mu_s}{\mu_{s,w}}\right)^{0.14} \quad (A.2)$$

As with $F_{ht,i}$, $F_{ht,o}$ was found for the shell side as described in Sinnott [68], κ_{wf} is the thermal conductivity of the working fluid, μ_s is the dynamic viscosity at the average shell's temperature between the inlet and outlet, while $\mu_{s,w}$ is working fluid's dynamic viscosity at the tube's outer wall temperature (i.e. the shell side) and d_s is the shell diameter as seen in Figure A.1:

$$d_s = d_B + d_{cl} = d_o\left(\frac{N_t}{K}\right)^n + d_{cl} \quad (A.3)$$

Where d_B is the tube bundle diameter, d_{cl} is the clearance between the shell and the tube bundle as given by Sinnott [68], N_t is the total number of tubes in the heat exchanger. The constants K and n were used to estimate the shell diameter and are dependent on pitch type, tube pitch (p_t) and number of tube passes. Values of K and n were taken from Sinnott [68]. The saturation section of the condenser has a different behaviour than a pure gas or liquid since it is a mixture of these two states. The U inside the condenser's two-phase section for the working fluid was calculated as shown in Equation (10), with the convective heat transfer ($h^*_{co,o}$) outside the tube given by:

$$h^*_{co,o} = 0.95\kappa_{wf}\left(\frac{\rho_l(\rho_l - \rho_v)gN_t l_t}{\dot{m}_{wf}}\right)^{0.33} \quad (A.4)$$

Where ρ_l and ρ_v are the working fluid densities as a saturated liquid and saturated vapour respectively, g is the gravitational acceleration assumed to be 9.81 m/s^2 and l_t stands for the tube's length. For $h^*_{co,i}$, the following expression was used:

$$h_{co,i}^{*} = \frac{\kappa_S Nu}{d_i} \quad (A.5)$$

The Nusselt number (*Nu)* was evaluated using the correlations given by Gnielinski [72].

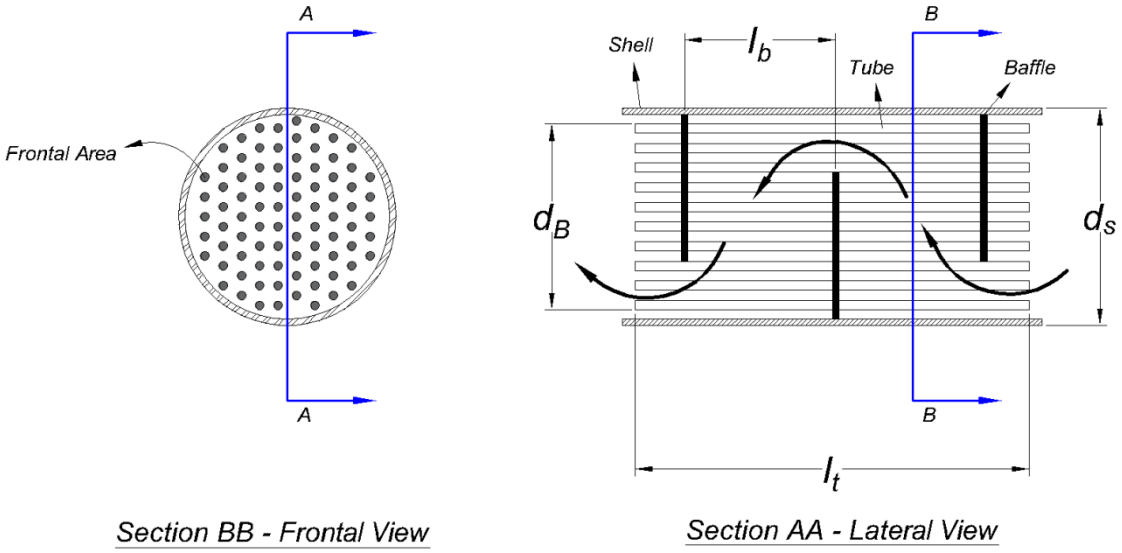

Figure A.1: Diagram that shows the important construction dimensions for the seawater condenser unit. Seawater runs inside the tubes while the working fluid flows in a non-ideal counter flow inside the shell. The figure is a simplified construction of a single tube pass inside a shell. The variable l_b stands for the baffle spacing, d_B is the tube bundle diameter, d_s is the shell diameter while l_t is the tube length. The grey area represents the heat exchanger seawater frontal area.

The pressure drop in the cooling fluid circuit (ΔP_i) was calculated as [68]:

$$\Delta P_i = \frac{N_t \rho_i v_i^2}{2}\left[8F_{f,i}\frac{l_t}{d_i}\left(\frac{\mu_s}{\mu_{w,s}}\right)^{-m} + 2.5\right] \quad (A.6)$$

Where v_i is the speed of the fluid inside the tube, $F_{f,i}$ is the correction factor due to friction inside the tube and was found in Sinnott [68], m had a value of 0.25 if the flow inside the tube is laminar (Re_d < 2,100) or 0.14 when it is turbulent (Re_d > 2,100). For the pressure drop in the working fluid side (ΔP_o) on the shell side was given by:

$$\Delta P_o = 4\rho v_o^2 F_{f,o}\left(\frac{d_s}{d_e}\right)\left(\frac{l_t}{l_b}\right)\left(\frac{\mu_s}{\mu_{w,s}}\right)^{-0.14} \quad (A.7)$$

Where v_o is the speed of the fluid in the shell side, $F_{f,o}$ is the friction factor for the shell circuit and found in Sinnott [68], d_e is the shell's hydraulic diameter and l_b is the distance between baffles. An alternative equation which allows to compare the power input from the pressure change device ($\dot{W}_S$) – seawater pump and air's fan – and its physical and performance characteristics was given by:

$$\dot{W}_S = \frac{v_i A_{cs} \Delta P_S}{\eta_S} \quad (A.8)$$

In the previous equation the change in pressure (ΔP_S) at the seawater pump is set to 100 kPa – to overcome the head losses from bringing the seawater from the waterline to where the condenser unit is located on board – plus the coolant pressure losses inside the condenser unit (ΔP_i). The seawater pump efficiency (η_S) was assumed to be 80% as with the working fluid pump. The cross-sectional area (A_{cs}) for a shell and tube heat exchanger where the coolant flows was given by:

$$A_{cs} = \frac{\pi N_t d_i^2}{4} \quad \text{(A.9)}$$

Where N_t is the total number of tubes. The condenser unit's volume (V) in a shell and tube heat exchanger was determined by:

$$V = \frac{\pi d_s^2 l_t}{4} \quad \text{(A.10)}$$

The condenser unit design was constrained to a maximum volume similar to a TEU shipping container (i.e. 38.5 m^3) which was considered to be enough space for the heat exchanger on board and with a minimal impact on the cargo capacity.

A.2 Finned Tube heat exchanger

Starting from the desuperheating section of the condenser unit, the convective heat transfer coefficient inside the tubes ($h^*_{ds,i}$) was found using Equation (A.5), while the heat transfer coefficient on the outside ($h^*_{ds,o}$) was given by:

$$h^*_{ds,o} = 0.38 \frac{\kappa_S}{d_o} Re^{0.6} Pr^{0.33} \left(\frac{A_{T,ds}}{A_{t,ds}}\right)^{-0.15} \quad \text{(A.11)}$$

Where κ_S is the air's thermal conductivity and Re was measured for the outside of the finned tubes. For the condensing section, $h^*_{co,o}$ was calculated using Equation (A.11) and for $h^*_{co,i}$ the following equation was used [86]:

$$h^*_{co,i} = 0.02273 \frac{\kappa_{wf} Nu \left(24.44 P_r^{19/50} + 89.91\right)}{d_i \, P_r^{19/50}} \quad \text{(A.12)}$$

Where P_r is the reduced pressure – P_3 divided by the working fluid's critical pressure (P_{cr}) – and Nu was found by the following expression:

$$Nu = 0.023 Re^{0.8} Pr^{0.4} \quad \text{(A.13)}$$

The pressure drop on the air side (ΔP_o) was found with:

$$\Delta P_o = 2 F_{f,o} \rho_S v_{os}^2 N_{tr} \quad \text{(A.14)}$$

Where v_{os} is the air's speed through the smallest cross-section of the tube bundle, ρ_S is the air's density, N_{tr} is number of tube rows, and $F_{f,o}$ is the friction factor on the air side found using the

Robinson and Briggs correlation for staggered tube bundles [87]. For the pressure drop inside the tubes (ΔP_i) – for the working fluid – the correlations from Gnielinski [72] and Müller-Steinhagen and Heck [75] were employed. The fan power can be determined by using Equation (A.8)), but in the case of the fan a constant η_S of 60% was used as suggested by Walraven et al. [88]. As seen in the work of Habl et al. [28] it can be expected that the air condenser unit's ΔP_S will impact considerably the fan power input. Hence, ΔP_S was minimised using a single variable optimisation available in Matlab® with the aim of reducing $\dot{W}_S$ [89]. The search space was between the atmospheric pressure and 106 kPa which ensure that the fan was capable of overcoming pressure losses and moving the air through the condenser unit.

The cross-sectional area of the air condenser (A_{cs}) as seen in Figure A.2 was found as follows:

$$A_{cs} = l_t p_t N_{tpr} \qquad \text{(A.15)}$$

Where l_t is the length of the tube, p_t is the tube's pitch and N_{tpr} are the number of tubes per row.

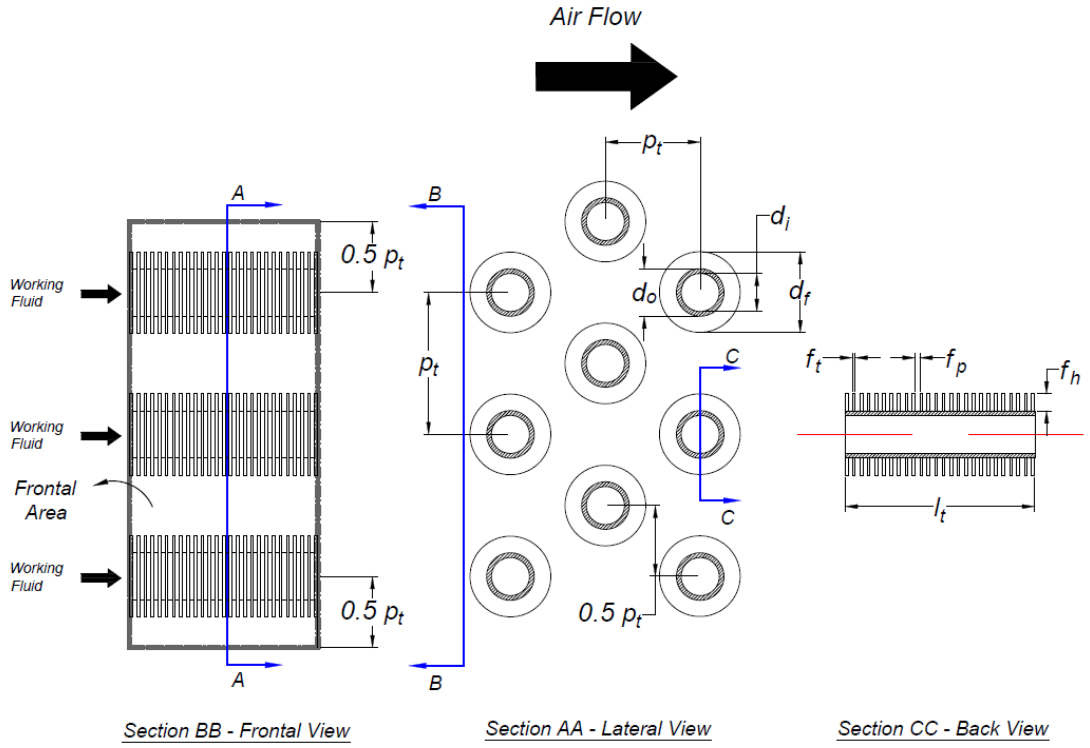

Figure A.2: Diagram that shows the different views of the finned tube heat exchanger. In the frontal view, the area covered by the grey square represents the heat exchanger cross-sectional area. The lateral view shows the tube layout for the marine WHRS cross-flow air condenser unit. Finally, the back view shows the fin thickness (f_t), pitch (f_p) and height (f_h) chosen by the optimisation process. The fin diameter is given by d_f.

In the case of the air condenser unit the volume was computed as follows:

$$V = p_t^2 l_t N_{tr} N_{tpr} \qquad \text{(A.16)}$$

Where N_{tr} represents the number of tube rows which for this paper was fixed to five. The maximum volume allowed also for this design was 38.5 m^3.

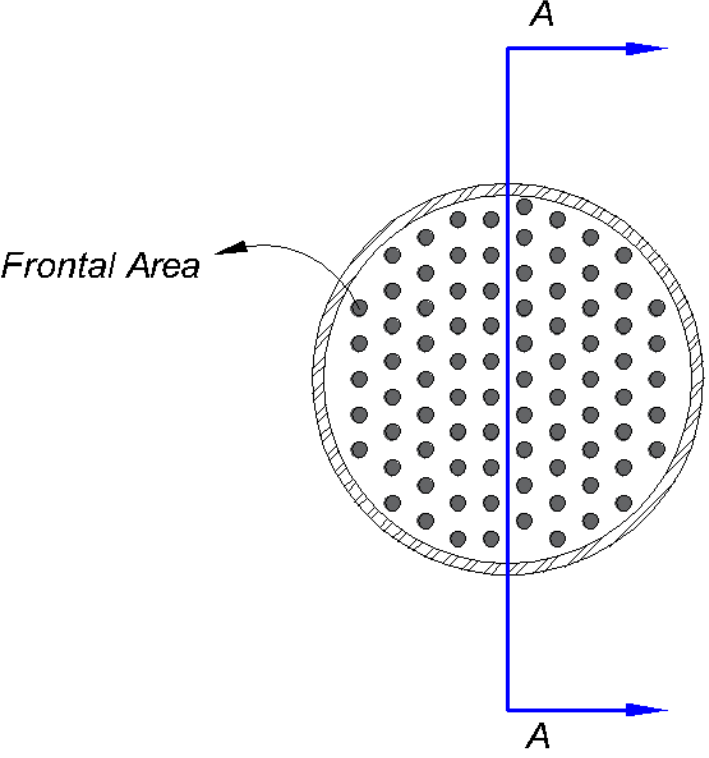

Section BB - Frontal View

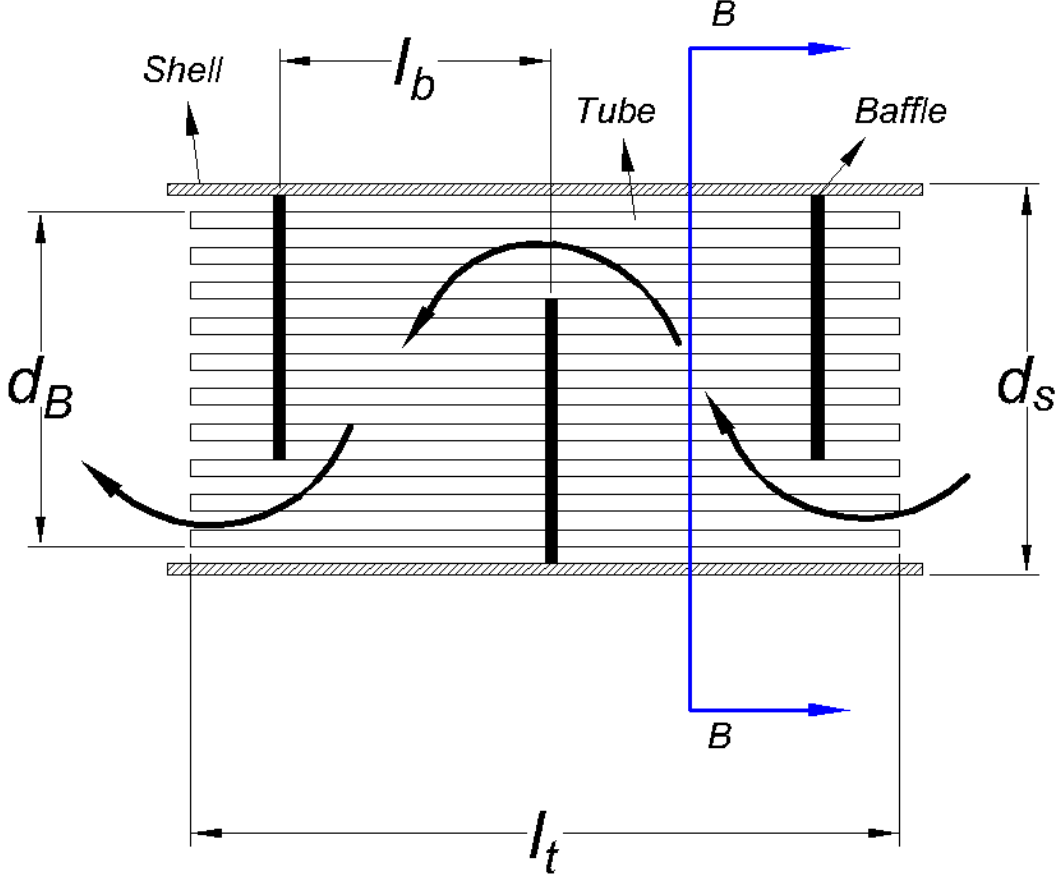

Section AA - Lateral View

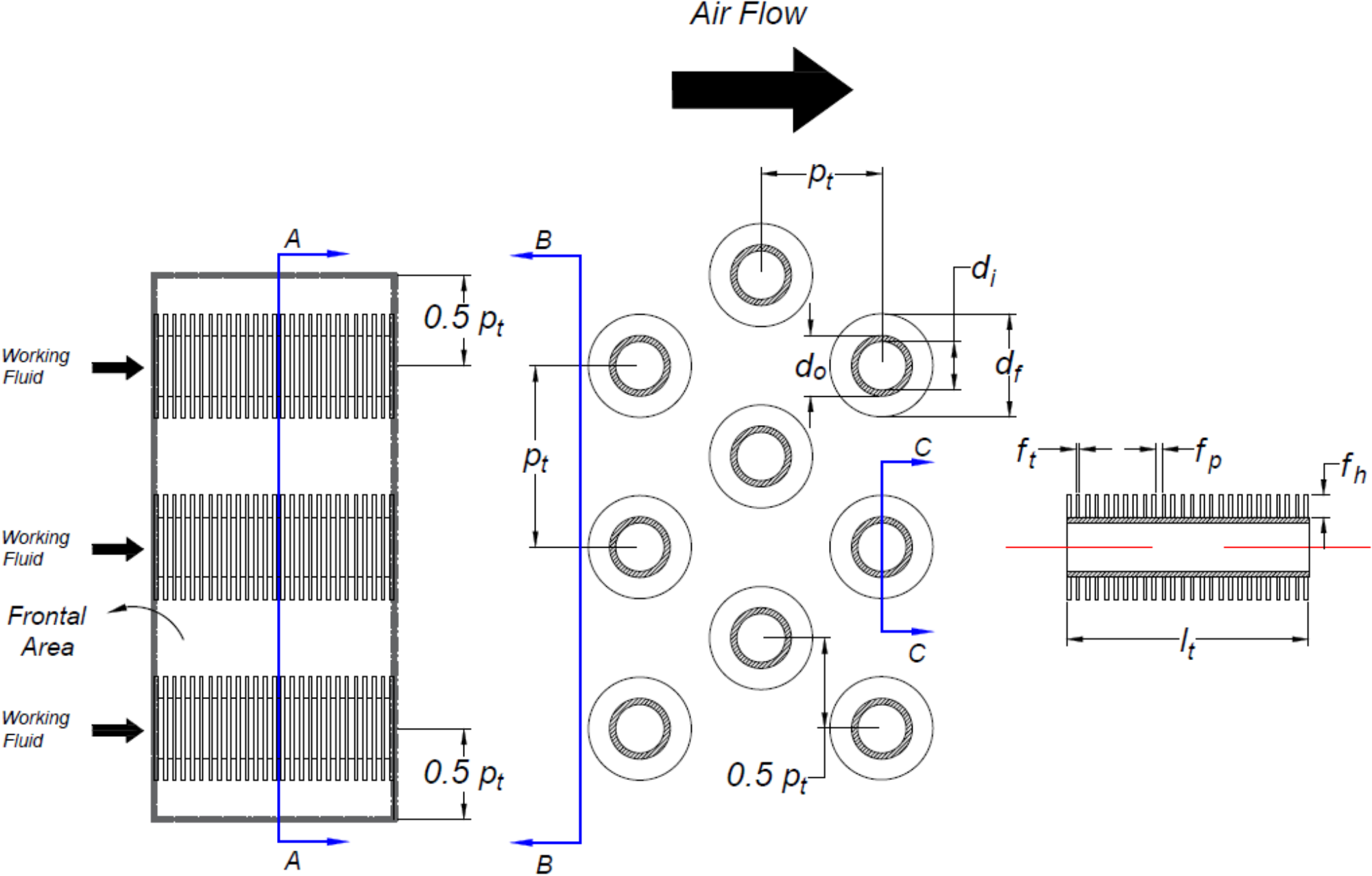

Section BB - Frontal View

Section AA - Lateral View

Section CC - Back View